

# Regulation of Thalamic and Cortical Network Synchrony by *Scn8a*

## Highlights

- Decreased *Scn8a* expression in cortical excitatory neurons reduces seizures
- Decreased *Scn8a* in the thalamic reticular nucleus (RT) leads to absence seizures
- Loss of *Scn8a* from RT cells preferentially impairs tonic firing mode behavior
- Loss of *Scn8a* impairs desynchronizing recurrent RT-RT synaptic inhibition

## Authors

Christopher D. Makinson,  
Brian S. Tanaka, Jordan M. Sorokin, ...,  
Alan L. Goldin, Andrew Escayg,  
John R. Huguenard

## Correspondence

aescayg@emory.edu (A.E.),  
john.huguenard@stanford.edu (J.R.H.)

## In Brief

Makinson et al. identify the mechanisms underlying the complex seizure phenotype associated with loss of the voltage-gated sodium channel *Scn8a*. *Scn8a*-mediated hypofunction in cortical circuits confers convulsive seizure resistance, while hypofunction in the thalamus is sufficient to generate absence seizures.



# Regulation of Thalamic and Cortical Network Synchrony by *Scn8a*

Christopher D. Makinson,<sup>1</sup> Brian S. Tanaka,<sup>2</sup> Jordan M. Sorokin,<sup>1</sup> Jennifer C. Wong,<sup>3</sup> Catherine A. Christian,<sup>1,4</sup> Alan L. Goldin,<sup>2</sup> Andrew Escayg,<sup>3,\*</sup> and John R. Huguenard<sup>1,5,\*</sup>

<sup>1</sup>Department of Neurology and Neurological Sciences, Stanford University, Stanford, CA 94304, USA

<sup>2</sup>Departments of Microbiology and Molecular Genetics and Anatomy and Neurobiology, University of California, Irvine, CA 92697, USA

<sup>3</sup>Department of Human Genetics, Emory University, Atlanta, GA 30322, USA

<sup>4</sup>Present address: Department of Molecular and Integrative Physiology, University of Illinois at Urbana-Champaign, Urbana, IL 61801, USA

<sup>5</sup>Lead Contact

\*Correspondence: [aescayg@emory.edu](mailto:aescayg@emory.edu) (A.E.), [john.huguenard@stanford.edu](mailto:john.huguenard@stanford.edu) (J.R.H.)

<http://dx.doi.org/10.1016/j.neuron.2017.01.031>

## SUMMARY

Voltage-gated sodium channel (VGSC) mutations cause severe epilepsies marked by intermittent, pathological hypersynchronous brain states. Here we present two mechanisms that help to explain how mutations in one VGSC gene, *Scn8a*, contribute to two distinct seizure phenotypes: (1) hypoexcitation of cortical circuits leading to convulsive seizure resistance, and (2) hyperexcitation of thalamocortical circuits leading to non-convulsive absence epilepsy. We found that loss of *Scn8a* leads to altered RT cell intrinsic excitability and a failure in recurrent RT synaptic inhibition. We propose that these deficits cooperate to enhance thalamocortical network synchrony and generate pathological oscillations. To our knowledge, this finding is the first clear demonstration of a pathological state tied to disruption of the RT-RT synapse. Our observation that loss of a single gene in the thalamus of an adult wild-type animal is sufficient to cause spike-wave discharges is striking and represents an example of absence epilepsy of thalamic origin.

## INTRODUCTION

Voltage-gated sodium channels (VGSCs) are critical mediators of neuronal excitability in all regions of the brain. They are primarily responsible for the initiation and propagation of action potentials but also shape neuronal activity via depolarizing subthreshold sodium currents (Bean, 2007; Raman and Bean, 1997; Raman et al., 1997; Taddese and Bean, 2002). As a result, mutations in VGSCs can have dramatic effects on neural circuit function. For example, mutations in all of the major CNS VGSC genes have been identified in patients with epilepsy (Claes et al., 2001; Escayg et al., 2000; Holland et al., 2008; Sugawara et al., 2001; Veeramah et al., 2012), a disorder of the CNS characterized by neuronal hyperexcitability and episodes of hypersynchrony. Recently, distinct seizure types, including generalized convulsive seizures and non-convulsive absence seizures, have been attrib-

uted to mutations in the VGSC gene *SCN8A* (Berghuis et al., 2015; Veeramah et al., 2012; Wagnon and Meisler, 2015). Alleles that reduce the activity of *Scn8a* are known to increase resistance to acute seizures, while also reducing seizure severity and improving survival of *Scn1a* epileptic mutant mice (Hawkins et al., 2011; Makinson et al., 2014; Martin et al., 2007). However, reduced *Scn8a* activity also leads to non-convulsive absence epilepsy in mice (Papale et al., 2009) and humans (Berghuis et al., 2015). Similarly, common antiepileptic drugs (AEDs) that act on VGSCs are known to effectively control generalized convulsive and partial epilepsies; however, they are often ineffective against absence seizures and may even increase the risk of absence epilepsy (Manning et al., 2003; Osorio et al., 2000; Posner, 2006).

Efforts to understand the relationship between *SCN8A* activity and seizure resistance have mainly focused on the role of this channel in the hippocampus, where increased expression is correlated with greater susceptibility to induced convulsive seizures (Blumenfeld et al., 2009) and reduced expression is associated with seizure resistance (Makinson et al., 2014). The relative contribution of different neuronal cell types to *SCN8A*-mediated seizure resistance is unknown and the etiology of *SCN8A*-absence epilepsy remains unexplored.

## RESULTS

### Distinct Excitatory and Inhibitory Cell Types Mediate *Scn8a* Seizure Protection and Absence Epilepsy

To identify the different neuronal populations that underlie *Scn8a*-associated seizure phenotypes, we first generated mouse lines in which *Scn8a* was deleted from select cell types and assessed seizure susceptibility and spontaneous electrographic activity. Mouse lines that express *Cre* recombinase in excitatory, inhibitory, or both neuronal cell types were crossed to animals carrying a floxed *Scn8a* allele (*Scn8a<sup>fl/+</sup>*) to produce offspring with selective heterozygous deletion of *Scn8a* (*Scn8a<sup>fl/+</sup>Cre*) and control animals lacking the *Cre* transgene (*Scn8a<sup>fl/+</sup>no-Cre*). Homozygous floxed *Scn8a* mice without *Cre* (*Scn8a<sup>fl/fl</sup>no-Cre*) were verified to have normal levels of *Scn8a* expression and normal susceptibility to flurothyl-induced seizures (Figure S1). Five *Cre* lines with different expression patterns were chosen to achieve inactivation of *Scn8a*: (1) broadly in the cerebral cortex (*FoxG1*) (Hébert and McConnell, 2000), (2) in glutamatergic excitatory

neurons (*Camk2a*, *Emx1*) (Dragatsis and Zeitlin, 2000; Gorski et al., 2002), (3) preferentially in inhibitory cells of the cortex, hippocampus, and striatum but not of the thalamic reticular nucleus (*Ppp1r2*) (Belforte et al., 2010), and (4) broadly in inhibitory cells throughout the brain (*Dlx5/6*) (Monory et al., 2006).

The susceptibility of mice with cell-type-specific deletion of *Scn8a* to chemically induced seizures was assessed by exposure to flurothyl (Makinson et al., 2016; Martin et al., 2007; Papale et al., 2009). *Scn8a<sup>fl/+</sup>FoxG1* animals (purple box) exhibited increased latencies to the generalized tonic clonic seizure (GTCS) but not to the initial myoclonic jerk (MJ), whereas *Scn8a<sup>fl/+</sup>* mice expressing either of the excitatory cell-specific *Cre* transgenes, *Emx1* or *Camk2a Cre* (blue box), exhibited increased latencies to both seizure behaviors (Figure 1; see Table S1 for statistics). By contrast, *Scn8a* deletion from inhibitory cells (red box) did not increase seizure latencies (Figure 1A; see Table S1 for statistics).

Homozygous floxed *Emx1 Cre* animals were also generated so that seizure latencies following complete deletion of *Scn8a* from excitatory cells could be assessed. Homozygous floxed *Emx1 Cre* (*Scn8a<sup>fl/fl</sup> Emx1*) animals did not display obvious behavioral abnormalities or reduced lifespan; however, these animals did exhibit increased seizure latencies over heterozygous deletions (Figure S3, MJ, *Scn8a<sup>fl/fl</sup> Emx1* 360 ± 26 s, *Scn8a<sup>fl/+</sup> Emx1* 309 ± 11 s *Scn8a<sup>fl/fl</sup> no-Cre* 275 ± 26 s; GTCS, *Scn8a<sup>fl/fl</sup> Emx1* 818 ± 14 s, *Scn8a<sup>fl/+</sup> Emx1* 681 ± 54 s *Scn8a<sup>fl/fl</sup> no-Cre* 491 ± 35 s).

Previously, we showed that globally reducing *Scn8a* activity reduced hippocampal hyperexcitability and seizure phenotypes associated with *Scn1a* epilepsy mutations (Hawkins et al., 2011; Makinson et al., 2014; Martin et al., 2007, 2010). To evaluate whether the deletion of *Scn8a* from excitatory neurons is sufficient to produce these effects, we evaluated hippocampal excitability in mice in which *Scn8a* was deleted from excitatory neurons. In hippocampal slices, the latency to high potassium-induced epileptiform bursts was elevated, while inter-burst frequency was reduced (Figures S4A and S4B, Latency, *Scn8a<sup>fl/+</sup> Emx1*, 7.4 ± 0.6 s versus *Scn8a<sup>fl/+</sup> no-Cre*, 4.6 ± 0.5 s; Frequency, *Scn8a<sup>fl/+</sup> Emx1*, 0.50 ± 0.04 Hz versus *Scn8a<sup>fl/+</sup> no-Cre*, 0.70 ± 0.04 Hz, Mann Whitney U test), while deletion in inhibitory cells had no effect (Figure S4B, Latency, *Scn8a<sup>fl/+</sup> Dlx5/6*, 4.3 ± 0.3 s versus *Scn8a<sup>fl/+</sup> no-Cre*, 4.4 ± 0.2 s; Frequency, *Scn8a<sup>fl/+</sup> Dlx5/6*, 0.78 ± 0.06 Hz versus *Scn8a<sup>fl/+</sup> no-Cre*, 0.72 ± 0.05 Hz, Mann Whitney U test,  $p > 0.05$ ). Hippocampal CA3 pyramidal cells from mice with excitatory-specific deletion (*Scn8a<sup>fl/+</sup> Emx1*) were less excitable, consistent with previous results with global *Scn8a* deletion (Royeck et al., 2008) (Figure S4D, number of action potentials [APs] in response to 150 pA current injection, *Scn8a<sup>fl/+</sup> Emx1*, 19.3 ± 0.5 versus *Scn8a<sup>fl/+</sup> no-Cre*, 27.7 ± 1.2, two-way ANOVA,  $p < 0.05$ ).

To evaluate *Scn8a*-associated seizure protection directly in a model of epilepsy, we generated mice carrying the *Scn1a*-R1648H genetic epilepsy with febrile seizures plus (GEFS+) mutation (Makinson et al., 2016; Martin et al., 2010) and excitatory cell-specific deletion of *Scn8a* as outlined in Figure S4E. Deletion was found both to increase seizure latencies and to normalize survival (Figure S4F; Seizure latencies, GTCS, *Scn8a<sup>fl/+</sup> no-Cre*, 443 ± 29 s, *Scn8a<sup>fl/+</sup> no-Cre Scn1a<sup>RH/+</sup>*, 332 ± 15 s, *Scn8a<sup>fl/+</sup> Emx1*, 714 ± 50 s, *Scn1a<sup>RH/+</sup> Scn8a<sup>fl/+</sup> Emx1*,

612 ± 43 s, One-way ANOVA, Dunnett's post hoc; Survival, *Scn8a<sup>fl/+</sup> no-Cre*, 9/9, 100%, *Scn8a<sup>fl/+</sup> Emx1*, 7/7, 100%, *Scn8a<sup>fl/+</sup> no-Cre Scn1a<sup>RH/+</sup>*, 8/12, 66.7%, *Scn1a<sup>RH/+</sup> Scn8a<sup>fl/+</sup> Emx1*, 8/8, 100%, Mantel-Cox test).

Global *Scn8a* loss leads to spontaneous absence seizures in mice (Papale et al., 2009). In order to determine whether selective loss of *Scn8a* from defined cell types is sufficient to generate absence seizures, mice from each of the five *Cre* crosses were instrumented for electrocorticogram (ECoG) recordings and 3 days of continuous records were analyzed (Figure 1B). Spontaneous absence seizures were only observed in mice in which *Scn8a* was deleted broadly in inhibitory cells (*Scn8a<sup>fl/+</sup> Dlx5/6*, absence seizures per day, 111 ± 23). Notably, restricting *Scn8a* deletion to select interneurons outside of the thalamus by the *Ppp1r2* transgene did not produce absence seizures (Figure 1B), and no other seizure types were observed in any of the other animals.

In order to make direct comparisons of chemi-convulsant sensitivity and absence seizure frequency between different cell-type-specific deletions on the same genetic background, mice expressing both the excitatory-specific *Emx1 Cre* and the inhibitory-specific *Dlx5/6 Cre* transgenes were generated and then crossed to *Scn8a<sup>fl/fl</sup>* mice as outlined in Figure 1C. This cross yielded offspring in which *Scn8a* was deleted in either excitatory (*Scn8a<sup>fl/+</sup> Emx1*), inhibitory (*Scn8a<sup>fl/+</sup> Dlx5/6*), or both (*Scn8a<sup>fl/+</sup> Emx1 Dlx5/6*) cell types, and control littermates that did not carry a *Cre* transgene (*Scn8a<sup>fl/+</sup> no-Cre*). Latencies to flurothyl-induced GTCS were found to be significantly increased in mice in which *Scn8a* was deleted in excitatory cells (*Scn8a<sup>fl/+</sup> Emx1*, GTCS, 639.8 ± 37.4 s) and in mice in which *Scn8a* was deleted in both excitatory and inhibitory cells (*Scn8a<sup>fl/+</sup> Emx1 Dlx5/6*, GTCS, 582.7 ± 36.5 s) when compared to control mice (*Scn8a<sup>fl/+</sup> no-Cre*, GTCS, 429.7 ± 30.4 s). In contrast, the average latency to the GTCS was not significantly altered in animals in which *Scn8a* was deleted from inhibitory cells (*Scn8a<sup>fl/+</sup> Dlx5/6*, GTCS, 359.0 ± 32.9 s) when compared to control mice (one-way ANOVA, Tukey post hoc,  $n = 7-9$  per genotype, Figure 1D). No absence seizures were detected during ECoG recordings in mice in which *Scn8a* was deleted from excitatory cells (*Scn8a<sup>fl/+</sup> Emx1*) or *Cre*-negative control (*Scn8a<sup>fl/+</sup> no-Cre*) animals (Figures 1E and 1F). However, frequent absence seizures were detected in mice in which *Scn8a* was deleted in inhibitory cells throughout the brain (Figures 1E-1F, *Scn8a<sup>fl/+</sup> Dlx5/6*, 79 ± 10 seizures per day). Interestingly, the frequency of absence seizures was significantly reduced in mice in which *Scn8a* was deleted in both excitatory and inhibitory cells (Figures 1E-1F, *Scn8a<sup>fl/+</sup> Emx1 Dlx5/6*, 20 ± 5 seizures per day) when compared to animals that only carried the inhibitory cell-specific *Dlx5/6 Cre* transgene (79 ± 10 seizures per day), indicating that reducing cortical excitability opposes absence seizure generation driven by loss of *Scn8a* from inhibitory cells (one-way ANOVA, Tukey post hoc,  $n = 7-9$  per genotype).

### **Scn8a Deficiency Leads to Thalamocortical Network Hypersynchrony In Vivo**

Absence seizures are a manifestation of hypersynchronous oscillations between cortical and thalamic structures. Thus, we evaluated spontaneous electrographic activity in the thalamocortical

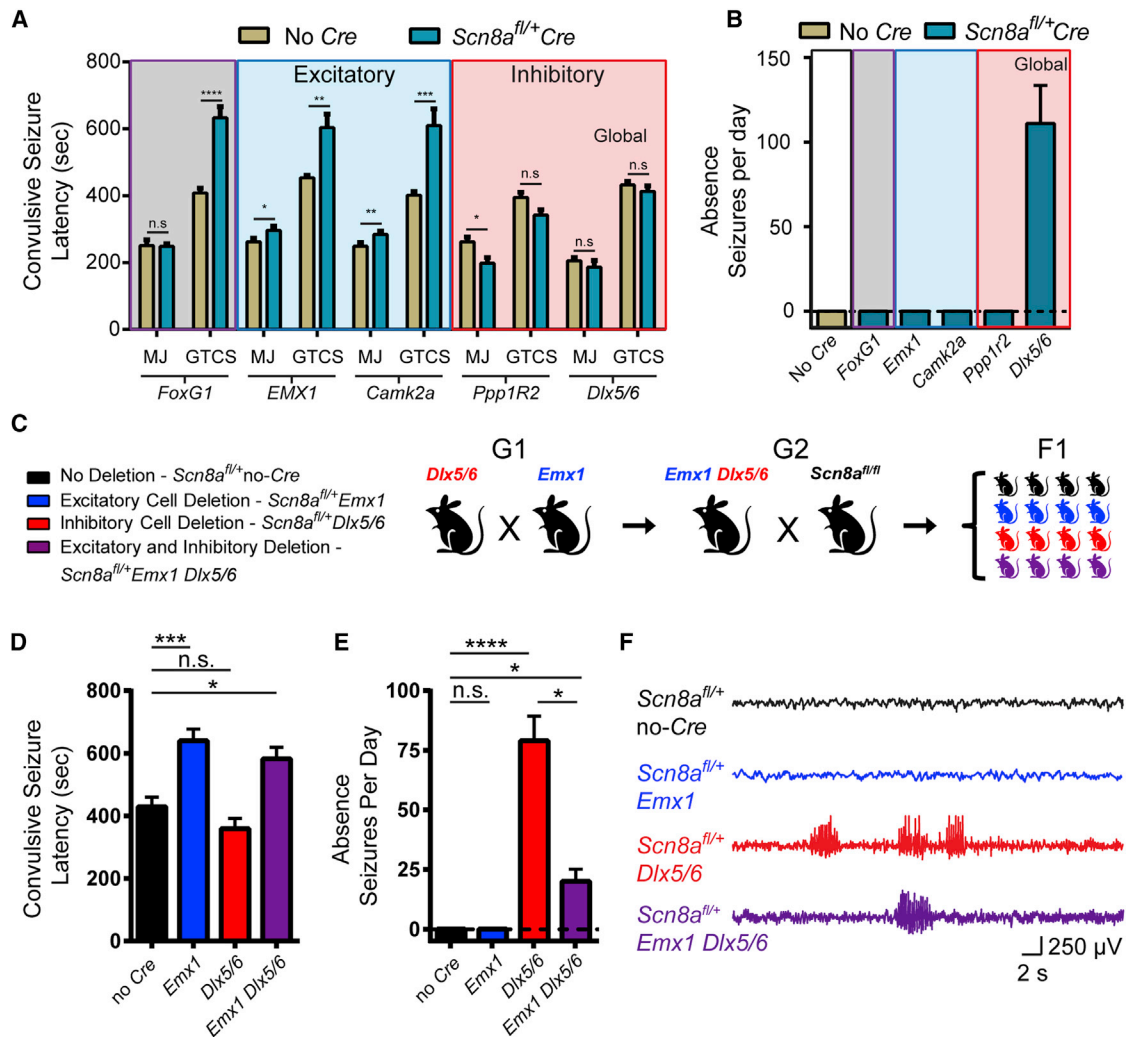


**Figure 1. Distinct Excitatory and Inhibitory Cell Types Mediate *Scn8a* Seizure Protection and Absence Epilepsy**

(A) *Scn8a* deletion in excitatory (blue box), but not inhibitory (red box), neurons increased convulsive seizure latency. Cell-type- and region-specific deletion of *Scn8a* was achieved by crossing *Cre* transgenic mouse lines to mice carrying a floxed *Scn8a* conditional allele. Susceptibility to flurothyl-induced seizures was determined by comparing the latency to two seizure behaviors; the myoclonic jerk (MJ) and generalized tonic-clonic seizure (GTCS). Littermate controls were used for all comparisons.  $n = 7$ –16 animals/genotype. See [Table S1](#) for statistics.

(B) Spontaneous absence seizures were measured by continuous 24 hr video/ECoG recordings. Broad inhibitory cell deletion by *Dlx5/6* *Cre* was sufficient to generate spontaneous absence seizures. Seizures were not observed in mice with deletion of *Scn8a* in the forebrain (*FoxG1*), excitatory cells (*Emx1* and *Camk2a*), or in inhibitory cells of the cortex, hippocampus, and striatum (*Ppp1r2*). One-way ANOVA,  $n = 4$ –5 animals/genotype.

(C) Schematic of breeding strategy to express both the excitatory and inhibitory cell-specific *Cre* transgenes within the same cross.

(D) Increased latencies to flurothyl-induced GTCS were observed in mice in which *Scn8a* was deleted from excitatory cells (*Emx1*) compared to *Cre*-negative littermate controls (no-*Cre*). One-way ANOVA,  $n = 7$ –9 animals/genotype.

(E) Spontaneous absence seizures were observed in animals with broad inhibitory cell deletion (red). Absence seizure generation was reduced following the additional deletion of *Scn8a* in cortical excitatory cells (purple). One-way ANOVA,  $n = 7$ –9 animals/genotype.

(F) Examples of ECoG recordings from each genotype.

(A–F) n.s.  $p > 0.05$ , \* $p < 0.05$ , \*\* $p < 0.01$ , \*\*\* $p < 0.001$ , \*\*\*\* $p < 0.0001$ .

See [Figures S1](#) and [S2](#) and [Tables S1](#) and [S2](#).

system of freely moving heterozygous null *Scn8a-med* mice (*Scn8a<sup>+/-</sup>*) (Kohrman et al., 1996). Recording electrodes were implanted at the surface of the cortex and tungsten wires were placed in somatosensory thalamus. All electrode positions were verified by histology after recordings. High-amplitude spike-wave discharges (SWDs) were recorded from cortical

and thalamic electrodes of all *Scn8a<sup>+/-</sup>* animals (Figure 2A) and detected using custom software (see STAR Methods). Seizures occurred at a frequency of  $0.88 \pm 0.16$  seizures per min and had an average duration of  $5.24 \pm 0.29$  s (Figure S5,  $n = 9$  animals). Peak spectral power of *Scn8a<sup>+/-</sup>* SWD events occurred at 7 Hz (Figure 2A, inset). Normalized power across five frequency bands

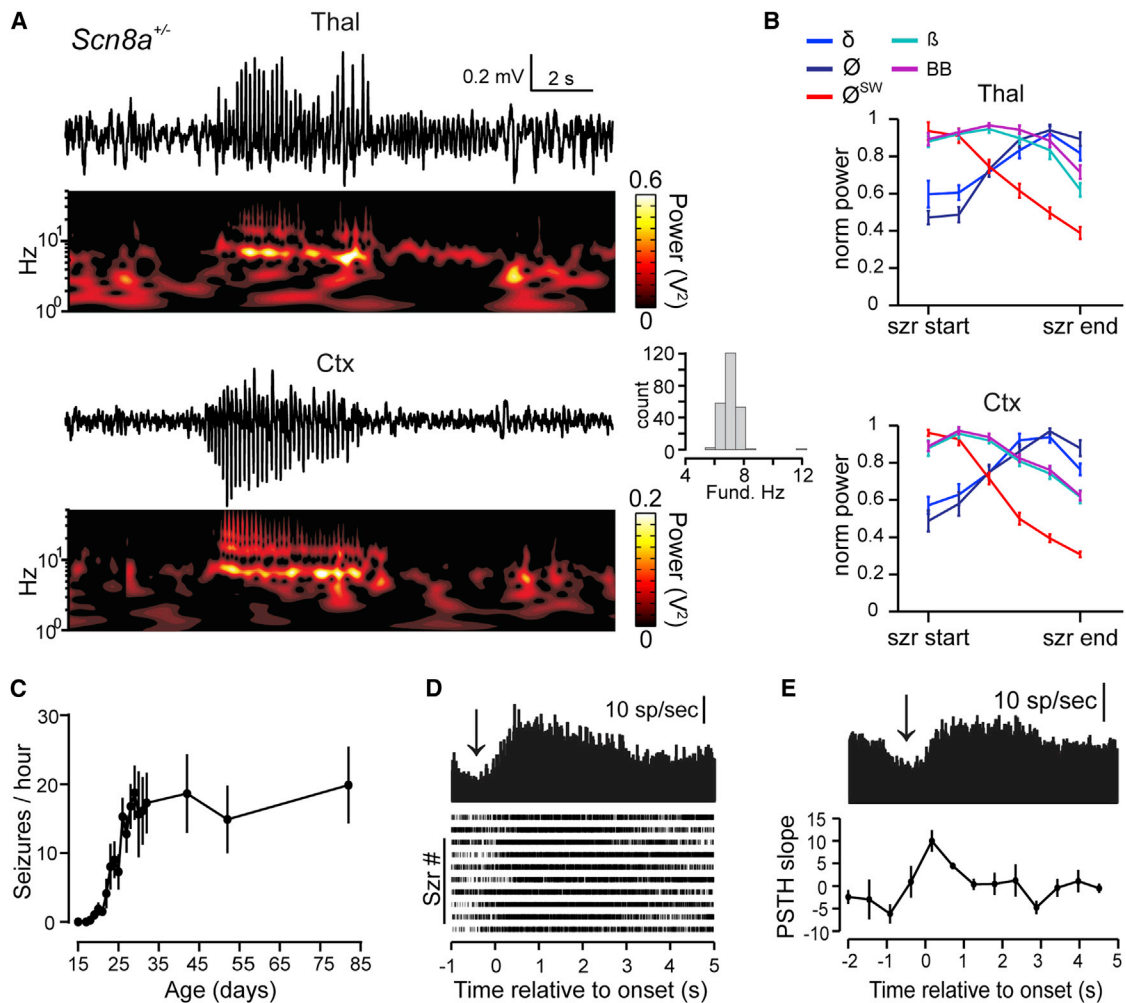


### Figure 2. *Scn8a* Deficiency Leads to Thalamocortical Network Hypersynchrony In Vivo

(A) Representative electrophysiological recordings of an absence seizure in the cortex and thalamus of an *Scn8a*<sup>+/-</sup> mouse. Peak spectral power of SWD events was measured at 7 Hz fundamental (Fund.) frequency in both the thalamus and cortex (inset).

(B) Each seizure (szr) was binned into six equally spaced segments and mean power was calculated for five frequency bands within each bin:  $\delta$  (2–4 Hz),  $\theta$  (4–7 Hz),  $\theta^{\text{SW}}$  (7–10 Hz),  $\beta$  (10–20 Hz), and broadband (BB, 2–20 Hz). Bands were normalized to their max values to capture the dynamics of each band over the duration of the seizure.  $n = 3$  animals.

(C) The developmental progression of seizure occurrence in *Scn8a*<sup>+/-</sup> mice was captured by video/ECOG monitoring spanning postnatal days 15 to 85. Seizures were first observed at day 17 and reached adult levels by the second postnatal month.  $n = 4$  animals.

(D and E) Spike rasters (D, bottom) and peri-stimulus time histograms (PSTHs) of multiunit (MU) activity surrounding ten seizures of one animal (D, top), and average PSTHs across animals (E, top). Linear regressions were fitted to the mean PSTHs over 500 ms intervals to obtain the average firing rate change throughout the duration of the seizure (E, bottom). Arrows indicate reduced thalamic firing preceding the onset of seizures (D and E).

See also Figure S5.

showed a progressive reduction in spike-wave ( $\theta^{\text{SW}}$ , 7–10 Hz) and increase in low-frequency ( $\delta$ , 2–4 Hz;  $\theta$ , 4–7 Hz) band power from the beginning to the end of the seizures (Figure 2B).

SWDs were first detected at postnatal day 17 and reached adult levels by the second postnatal month in *Scn8a*<sup>+/-</sup> animals (Figure 2C). This increase in the frequency of SWDs during postnatal development coincides with previously described developmental increases in Na<sub>v</sub>1.6 levels (protein product of *Scn8a*) (Makinson et al., 2014).

Multiunit activity collected from the somatosensory thalamus revealed a robust and prolonged (~1 s) decrease in firing rate

that preceded the onset of SWDs (Figures 2D and 2E). This pre-seizure reduction of thalamic multiunit activity was consistently observed between seizures in the same animal (Figure 2D) and between different animals (Figure 2E).

### Isolated Thalamic Circuits of *Scn8a*-Deficient Animals Display Increased Spontaneous and Evoked Oscillatory Activity

Our observation that deletion of *Scn8a* broadly in interneurons but not by a *Cre* line that targets inhibitory cells outside of the thalamus is sufficient to cause absence seizures (Figure 1) and

the observation that *Scn8a* absence seizures involve strong thalamic activity and changes in thalamic pre-seizure state (Figure 2), motivated an evaluation of *Scn8a* channel expression in inhibitory cells of the thalamus. *Scn8a* expression was previously identified in some subpopulations of cortical interneurons (Lorincz and Nusser, 2008); however, expression in thalamic inhibitory cells was unknown. We therefore performed immunohistochemistry for *Scn8a* and the inhibitory marker GAD65/67 in mouse brain slices and counted the percentage of double-labeled *Scn8a* processes. Consistent with previous findings, we found evidence for the expression of *Scn8a* in axons in cortical inhibitory cells (5.6% of *Scn8a* segments colocalized with GAD65/67,  $n = 3$  animals, Figures 3A and 3B) (Lorincz and Nusser, 2008; Makinson et al., 2016). GAD65/67-negative *Scn8a* processes that predominate in the cortex likely represent axon initial segments (AISs) of excitatory projection neurons as previously described (Lorincz and Nusser, 2008). By contrast, a high percentage of *Scn8a* processes in the thalamic reticular nucleus (RT) were found to be positive for GAD65/67 (71.7% GAD65/67- and *Scn8a*-positive processes,  $n = 3$  WT animals), while few *Scn8a*-positive RT processes were GAD65/67-negative (28.3% GAD65/67-negative *Scn8a* processes,  $n = 3$ , Figures 3A and 3B).

In order to evaluate the functional consequence of loss of *Scn8a* on thalamic synchronization, we made thalamic slice preparations as previously described (Huntsman et al., 1999) and measured spontaneous and evoked oscillatory activity. This slice preparation maintains an isolated thalamic circuit that contains reciprocally connected RT and TC cells (Figure 3C). This nested thalamic oscillator has been shown to be centrally involved in the generation and maintenance of absence seizures (Huntsman et al., 1999; Kleiman-Weiner et al., 2009; Paz et al., 2011; Steriade et al., 1993). We found that 56% of thalamic slices from *Scn8a*<sup>+/-</sup> animals display spontaneous oscillatory activity, while spontaneous oscillations were not observed in WT slices (Figure 3E). Compared to WT slices, evoked oscillations in *Scn8a*<sup>+/-</sup> slices were longer in duration and involved a greater number of bursts (Duration, WT,  $1.8 \pm 0.7$  s, *Scn8a*<sup>+/-</sup>,  $6.9 \pm 1.5$  s; Burst number, WT,  $12.1 \pm 4.5$ , *Scn8a*<sup>+/-</sup>,  $50.9 \pm 13.0$ ,  $n = 8-9$  slices/group; Figures 3F-3J). Though bursts were fewer in number in WT animals, the oscillation burst frequency was not different between WT and *Scn8a*<sup>+/-</sup> slices (WT,  $7.4 \pm 0.7$  Hz, *Scn8a*<sup>+/-</sup>,  $8.2 \pm 0.6$  Hz, Figure 3K).

### **Scn8a-Dependent Deficits in RT Spike Firing Preferentially Affect Tonic Firing Modes**

Having observed increased thalamic network synchrony in vivo and in vitro, we next evaluated the intrinsic properties of thalamic neurons of *Scn8a*<sup>+/-</sup> animals and animals in which *Scn8a* was deleted from inhibitory cells (*Scn8a*<sup>fl/+Dlx5/6</sup>). Depolarizing current steps were used to evoke sustained trains of action potentials (Tonic) while rebound bursts (Reb. Burst) were evoked by steps of hyperpolarizing current in RT (Figure 4A) and thalamocortical (TC) (Figure 4B) cells. We found that RT cells of *Scn8a*<sup>+/-</sup> mice produced fewer APs in both tonic and burst firing modes (Figure 4C1). In contrast, the number of tonic and burst APs was not altered in TC cells (Figure 4D1). Instantaneous firing frequency was reduced in tonic but not burst firing modes of

RT cells (Figure 4C2), while instantaneous firing frequency of TC cells was not affected (Figure 4D2). In order to directly compare the relative consequences of reduced *Scn8a* expression on burst versus tonic firing modes, we performed burst index (BI) calculations as detailed in the STAR Methods section. Briefly, BI is a composite measure reflecting the currents required to generate tonic versus rebound APs and the frequency of generated APs in each case. Increased BI values indicate increased burst versus tonic firing, while decreased BI values indicate increased tonic versus burst firing. RT cells of *Scn8a*<sup>+/-</sup> slices were found to exhibit increased BI compared to WT while TC cells were not affected (BI, RT, WT,  $0.45 \pm 0.03$ , versus *Scn8a*<sup>+/-</sup>,  $0.59 \pm 0.03$ ; TC, WT,  $0.81 \pm 0.04$ , versus *Scn8a*<sup>+/-</sup>,  $0.83 \pm 0.03$ ; Figure 4E).

In order to evaluate the firing properties of RT cells in mice in which *Scn8a* was deleted in inhibitory cells by the *Dlx5/6-Cre* transgene, we performed current-clamp recordings and analyzed responses to depolarizing and hyperpolarizing current steps (Figure 4G). tdTomato reporter expression was used to aid the identification of *Cre*-positive RT cells (Figure 4F). Reduced tonic and burst APs were observed in *Scn8a*-deleted RT cells compared to *Cre*-negative control mice (Figure 4H). We then performed BI calculations using these voltage recordings and, similar to our findings in *Scn8a*<sup>+/-</sup> animals, we found that the RT cells of mice in which *Scn8a* was deleted in interneurons exhibit increased BI compared to *Cre*-negative controls (BI, RT, Control,  $0.33 \pm 0.03$ , versus Deleted,  $0.45 \pm 0.04$ ; Figure 4I).

### **Loss of Scn8a Impairs Intra-RT Inhibition but Not RT → TC Inhibition**

Deficits in RT cell excitability and AP generation in *Scn8a*<sup>+/-</sup> animals are predicted to affect synaptic outputs of RT cells. To make comparisons of RT synaptic responses at RT and TC cells in WT and *Scn8a*<sup>+/-</sup> animals, we developed a cell-type-specific assay of RT synaptic output that employs ultrafast channelrhodopsin (ChETA) (Gunaydin et al., 2010) activation of RT cells and/or their axons (Figures S6B and S6C) with concurrent intracellular measurement of evoked inhibitory postsynaptic currents (eIPSCs) in TC or RT cells (Figures S6D and S6E). Adeno-associated virus containing a *Cre*-dependent ChETA-YFP construct was injected into the RT of WT and *Scn8a*<sup>+/-</sup> animals carrying a parvalbumin-*Cre* transgene. This technique achieved highly specific RT ChETA expression (Figure S6A). Viral targeting of ChETA-YFP was evaluated immediately following brain slicing and slices were fixed after recordings for immunostaining and imaging (Figure S6A). Using this assay, we found that RT → TC synaptic inhibition is robust across a range of stimulation frequencies and unaltered by partial loss of *Scn8a* (Figures 5D and 5F, two-way ANOVA,  $p > 0.05$ ,  $n = 5-9$  per genotype; Figures S6F and S6G). In contrast, *Scn8a*<sup>+/-</sup> RT → RT eIPSCs exhibited increased activity-dependent failure when compared to WT RT → RT eIPSCs (Figures 5D and 5E, two-way ANOVA, Tukey post hoc,  $*p < 0.05$ ,  $**p < 0.01$ ,  $n = 5-11$  per genotype; Figures S6F and S6G).

### **Selective RNAi Knockdown of Scn8a in RT Is Sufficient to Generate Absence Seizures**

Our findings implicate RT neurons in the pathophysiology of *Scn8a*<sup>+/-</sup> absence epilepsy. Therefore, to determine whether

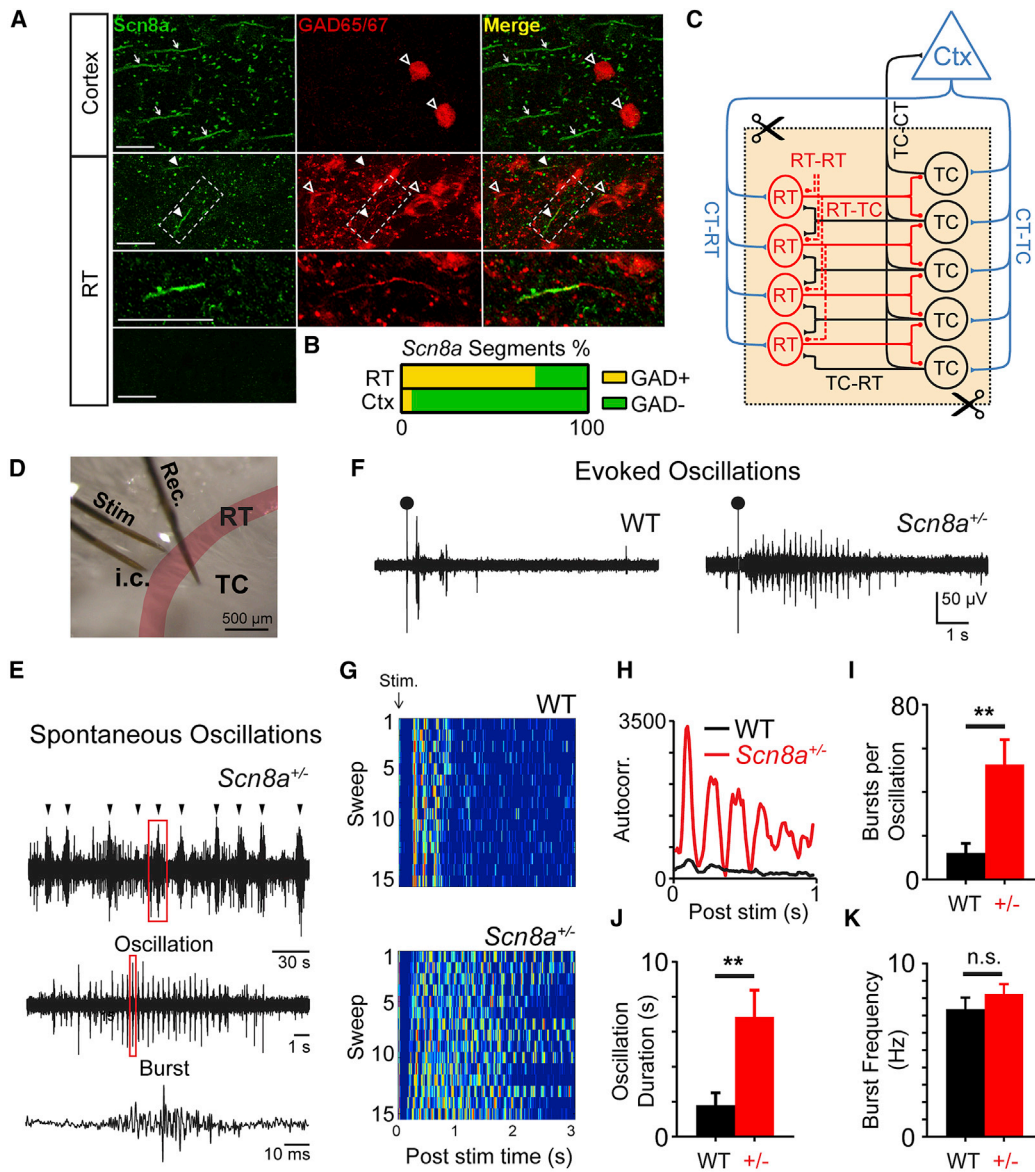


**Figure 3. Isolated Thalamic Circuits of *Scn8a*-Deficient Animals Display Increased Spontaneous and Evoked Oscillatory Activity**

(A) *Scn8a* and GAD65/67 immunoreactivity in the cortex and RT. Dashed box indicate regions of colocalization expanded below. Bottom: lack of *Scn8a* immunoreactivity in *Scn8a*<sup>-/-</sup> negative control tissue. Arrows indicate *Scn8a*-positive processes that are negative for cell-type marker. Open arrowheads indicate GAD65/67-positive cell bodies. Closed arrowheads indicate colocalization. Scale bars, 10  $\mu$ m. n = 3 animals.

(B) Percentage of *Scn8a*-positive processes in RT and cortex that are GAD65/67 positive (yellow) and negative (green).

(C) Diagram of the rhythmic thalamocortical circuitry isolated by the slice preparation (shaded).

(D) Image of the thalamic interface slice preparation. Electrical stimulation is applied to the internal capsule (i.c.) while recording extracellular multiunit activity in TC nuclei.

(E) Spontaneous oscillations were observed in thalamic slices of *Scn8a*<sup>+/-</sup> mice, with each oscillation composed of periodic bursts of spikes. No spontaneous oscillations were observed in WT littermates.

(F) Representative examples of evoked multiunit responses of *Scn8a*<sup>+/-</sup> and WT mice. Black circle indicates the stimulation artifact.

(G) Peristimulus time histograms (PSTHs) for spikes in WT and *Scn8a*<sup>+/-</sup> slices for 15 sequential evoked responses show increased duration of phasic spiking activity in *Scn8a*<sup>+/-</sup> mice compared to WT controls. Color intensity codes number of spikes in each time bin, showing repeated cycles of oscillations lasting for ~3 s in *Scn8a*<sup>+/-</sup> versus < 1 s in WT.

(H) Autocorrelograms derived from PSTHs of representative *Scn8a*<sup>+/-</sup> and WT evoked oscillations.

(I) Number of bursts per oscillation are increased in *Scn8a*<sup>+/-</sup> slices.

(J) Duration of oscillations is increased in *Scn8a*<sup>+/-</sup> slices.

(K) No significant differences in inter-burst oscillation frequency was observed between WT and *Scn8a*<sup>+/-</sup> slices.

(I–K) n.s. p > 0.05, \*\*p < 0.01, Mann Whitney U test, n = 8–9 slices/group; 5 animals/group.

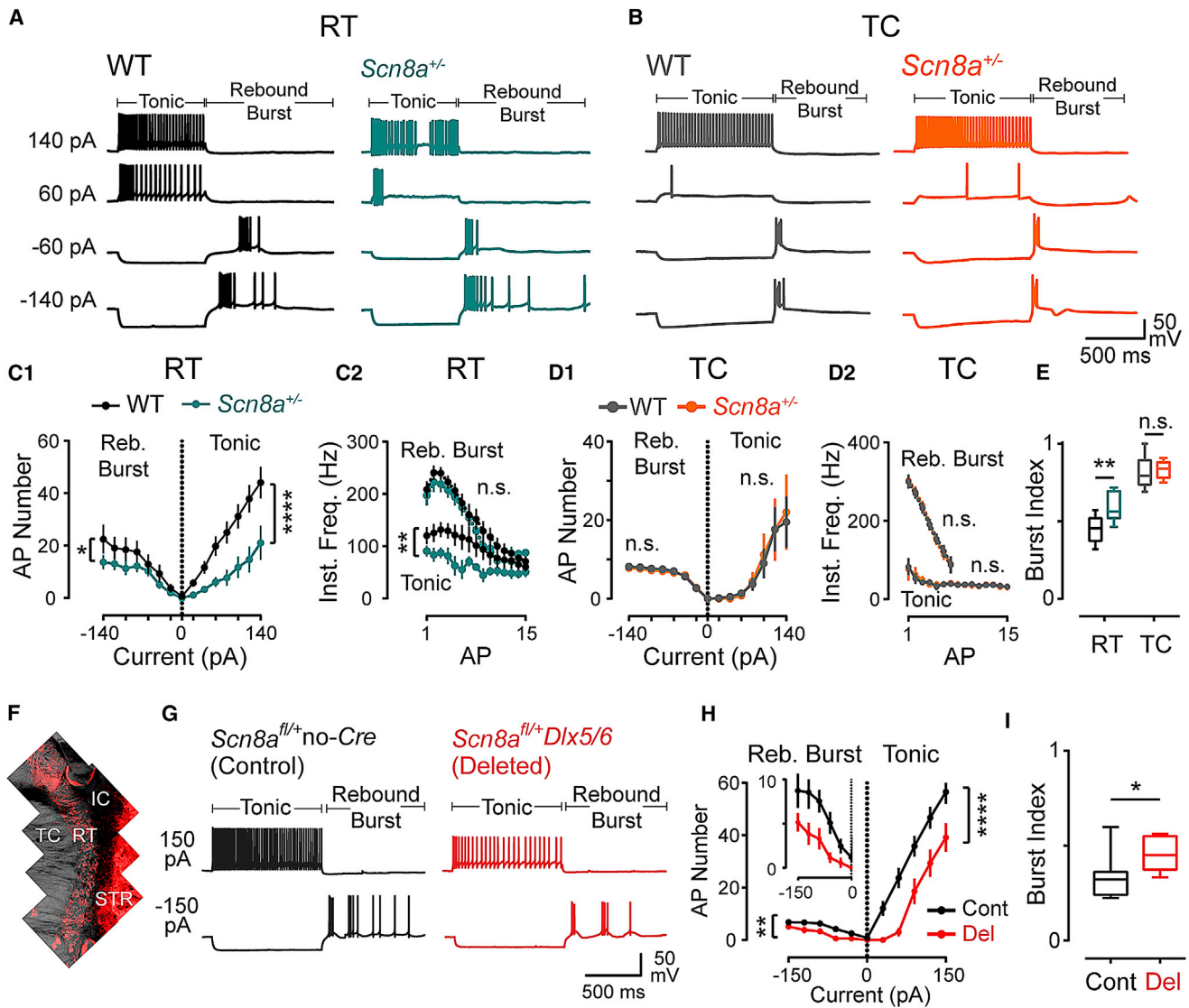


**Figure 4. *Scn8a*-Dependent Deficits in RT Spike Firing Preferentially Affect Tonic versus Burst Firing Modes**

(A and B) Intracellular voltage recordings from WT and *Scn8a*<sup>+/-</sup> RT (A) and TC (B) neurons.

(C1) Impaired tonic and rebound burst (Reb. Burst) AP generation was observed in *Scn8a*<sup>+/-</sup> compared to WT RT cells. Two-way ANOVA, n = 9 cells per group, 6 animals/group, 1–2 slices/animal.

(C2) Reduced instantaneous frequency was observed in tonic but not rebound burst modes of AP firing in *Scn8a*<sup>+/-</sup> compared to WT RT cells. n = 9 cells/group, 6 animals/group, 1–2 slices/animal.

(D1 and D2) No change in tonic or rebound burst AP number or instantaneous frequency was observed in *Scn8a*<sup>+/-</sup> versus WT TC cells. Two-way ANOVA, n = 5–6 cells/group, 4–5 animals/group, 1–2 slices/animal.

(E) Rebound burst versus tonic AP generation was compared using burst index. *Scn8a*<sup>+/-</sup> RT, but not TC, cells exhibited increased burst index values compared to WT cells. Mann-Whitney U test, n = 5–9 cells/genotype, 4–6 animals/group, 1–2 slices/animal.

(F) Identification of *Dlx5/6*-Cre-positive RT cells for patch-clamp physiology was aided by the presence of Cre-dependent tdTomato fluorescent reporter expression (red), Mann-Whitney U test, n = 5–7 cells/genotype.

(G) Representative images of voltage responses to depolarizing and hyperpolarizing current injection, *Scn8a*<sup>fl/+</sup> no-Cre control (black), and *Scn8a*<sup>fl/+</sup> *Dlx5/6*-deleted (red) animals.

(H) *Scn8a*<sup>fl/+</sup> *Dlx5/6* cells exhibited reduced rebound burst and tonic AP generation.

(I) *Scn8a*<sup>fl/+</sup> *Dlx5/6* RT cells exhibited increased burst index values compared to no-Cre controls. Mann-Whitney U test, n = 5–7 cells/genotype.

(C–I) Littermate controls were used for all comparisons. n.s. p > 0.05, \*p < 0.05, \*\*p < 0.01, \*\*\*p < 0.001, \*\*\*\*p < 0.0001, error bars represent ± SEM.

loss of *Scn8a* from RT cells is sufficient to generate absence seizures in WT animals, we constructed short hairpin RNA (shRNA) constructs representing sequences directed against *Scn8a* or a

scrambled control (AAV-shRNA-*Scn8a*-GFP or AAV-shRNA-Scram-GFP, respectively). We first validated the efficiency of *Scn8a* knockdown and specificity of knockdown for *Scn8a*

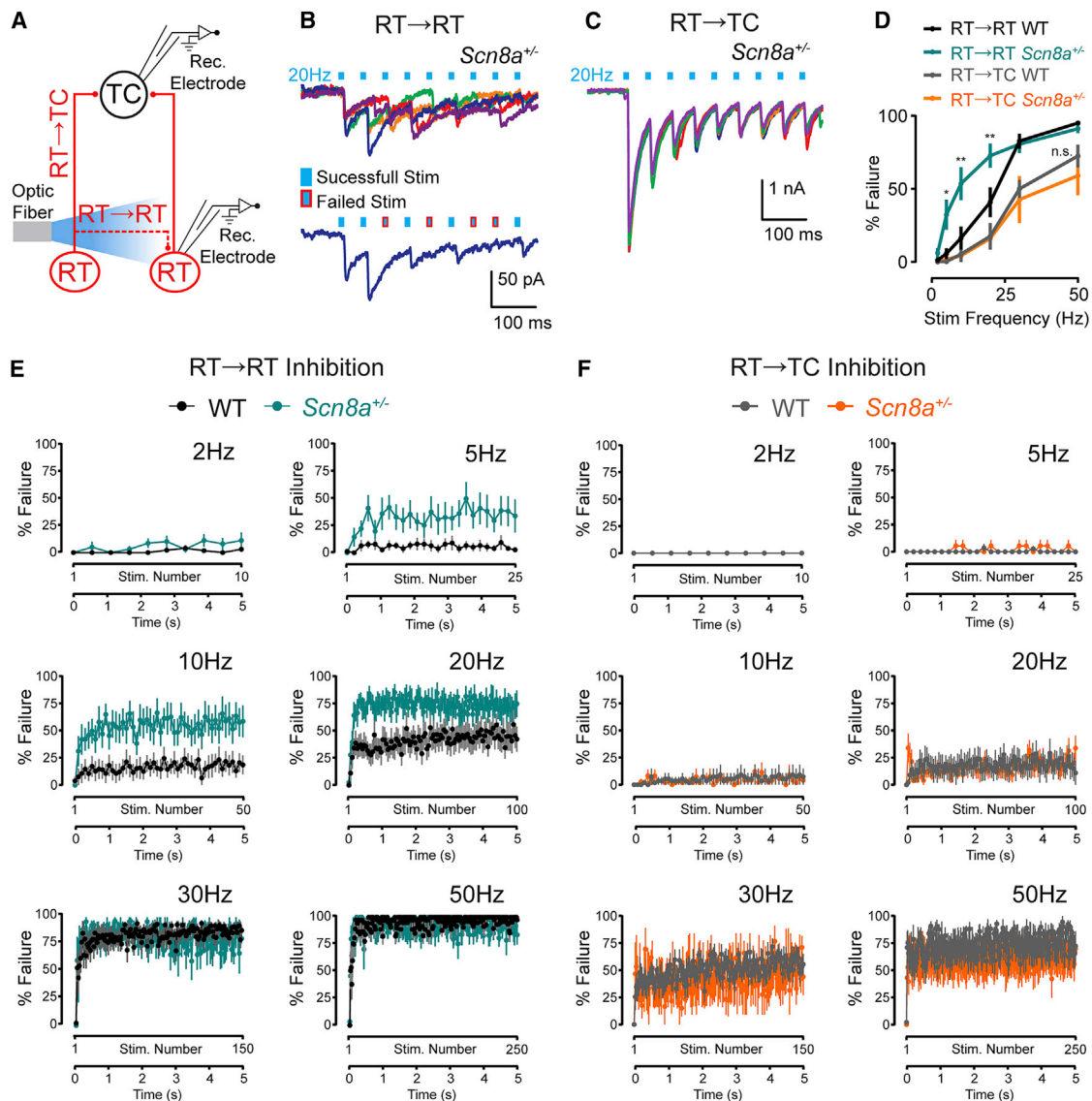


**Figure 5. Loss of *Scn8a* Impairs Intra-RT but Not RT  $\rightarrow$  TC Inhibition**

(A) Schematic of the isolated RT synaptic targets in the dorsal thalamus and experimental manipulation of RT activity. Activation of RT cells was achieved by injection of a viral construct containing the Cre-dependent ultrafast channelrhodopsin variant ChETA into the dorsal thalamus of *Scn8a*<sup>+/-</sup> and WT animals that carried a parvalbumin-(PV) specific Cre transgene (*Scn8a*<sup>+/-</sup>-PV-Cre and *Scn8a*<sup>+/+</sup>-PV-Cre). Blue light (2 ms, 20 mW power, 475 nm) pulses were applied under conditions of glutamate blockade (kynurinic acid, 1 mM) to eliminate contamination of eIPSCs by recurrent feedback from intrathalamic excitatory synaptic activity. ChETA-evoked IPSCs in RT (red ovals) and TC (black circle) cells were measured by whole-cell voltage-clamp recordings.

(B) Examples of 20 Hz ChETA stimulations in a *Scn8a*<sup>+/-</sup> RT cell. Isolated sweep (bottom, dark blue) shows stimuli within train that either evoked a synaptic response (blue boxes) or failed to do so (blue box with red border). Overall, responses were quite variable, with many failures on each trial.

(C) Examples of *Scn8a*<sup>+/-</sup> TC cell responses to ChETA activation of RT cells. TC cells reliably displayed eIPSCs at 20 Hz, with limited short-term depression that was very consistent between trials.

(D) *Scn8a*<sup>+/-</sup> RT synapses displayed enhanced frequency-dependent IPSC failures (above 2 Hz) compared to control littermates. No significant differences in RT  $\rightarrow$  TC IPSC failures were observed. n.s.  $p > 0.05$ , \* $p < 0.05$ , \*\* $p < 0.01$ , two-way ANOVA, Tukey post hoc,  $n = 8$ –11 cells/group, 6–8 animals/group, 1 cell/slice.

(E) Percent failure of RT  $\rightarrow$  RT synaptic inhibition with increasing stimulation frequencies in WT and *Scn8a*<sup>+/-</sup> slices.

(F) Percent failure of RT  $\rightarrow$  TC synaptic inhibition with increasing stimulation frequencies in WT and *Scn8a*<sup>+/-</sup> slices.

(E and F) Percent failure at each stimulation over 5 s is displayed for each stimulus frequency (2, 5, 10, 20, 30, and 50 Hz).  $n = 8$ –11 cells/group, 6–8 animals/group, 1 cell/slice.

See also Figure S6.

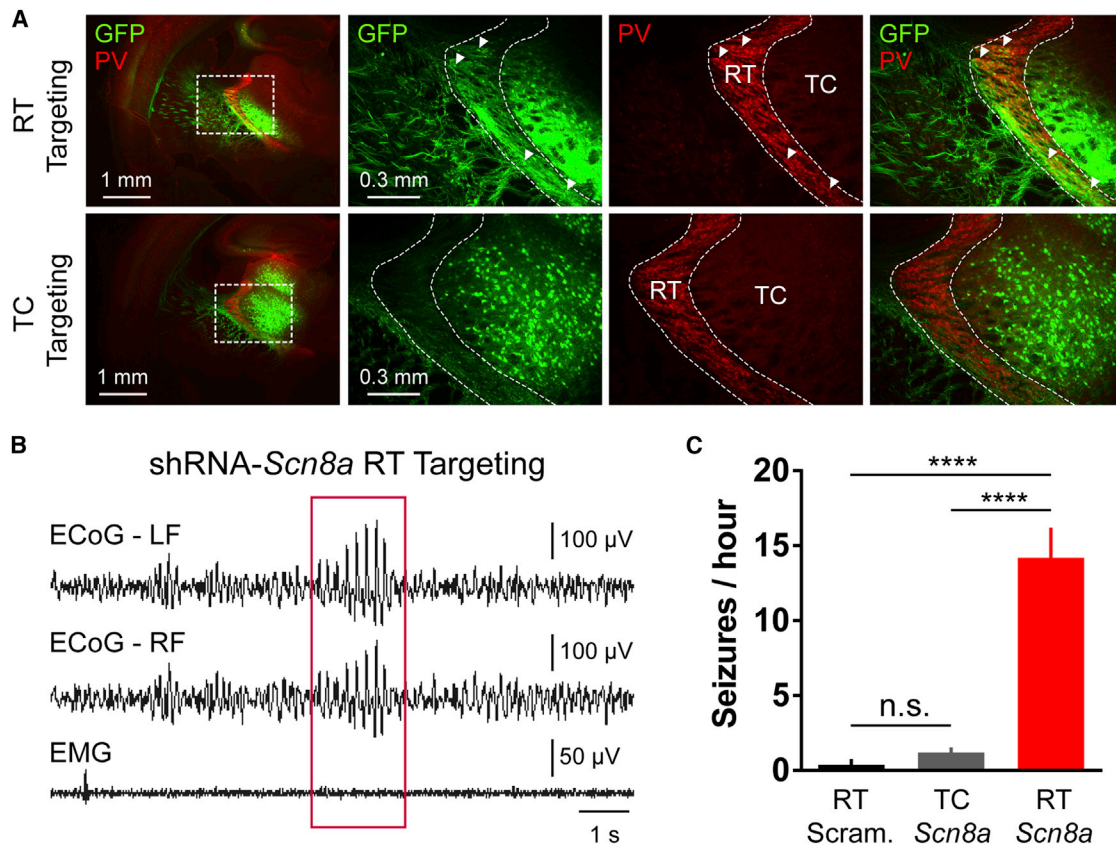


### Figure 6. Selective RNAi Knockdown of *Scn8a* in RT Is Sufficient to Generate Absence Seizures

(A) Images of selective targeting of AAVs in RT and TC regions of the thalamus. To delineate the boundaries of RT (dashed lines), parvalbumin was immunolabeled (red), while the area in which virus is expressed is marked by GFP (green). The dashed box in the leftmost panel shows the inset region that is magnified in the remaining panels. Arrowheads indicate selected double-labeled cell bodies in RT. Note that while specific TC targeting was possible, RT targeting also included some TC cells.

(B) Example ECoG traces (left and right hemispheres) of an absence seizure from a WT mouse targeted with the shRNA-*Scn8a*. Red box indicates the absence seizure.

(C) Quantification of detected absence seizures following injection of either shRNA-Scram in RT, shRNA-*Scn8a* in TC, or shRNA-*Scn8a* in RT (one-way ANOVA, Tukey post hoc, n.s.  $p > 0.05$ , \*\*\*\* $p < 0.0001$ ,  $n = 4-5$  animals/group).

See also Figure S7.

versus the other VGSC  $\alpha$  subunits that are highly expressed in the adult brain via western blot analysis (Figure S7). AAV-shRNA-*Scn8a*-GFP (shRNA-*Scn8a*) reduced *Scn8a* expression in the targeted region by approximately 65% compared to AAV-shRNA-Scram-GFP (shRNA-Scram), while no significant change in expression levels of  $\text{Na}_v1.1$  (*Scn1a*) or  $\text{Na}_v1.2$  (*Scn2a*) were observed (Figure S7). AAV constructs encoding either shRNA-*Scn8a* or shRNA-Scram were injected into the RT and TC regions of the thalamus (Figure 6A) and the animals were instrumented for cortical ECoG recordings. Three weeks after injection, 24 hr of continuous ECoG recordings were analyzed for the presence of seizure activity. No significant differences in seizure frequency were observed between light and dark periods. Frequent absence seizures were observed in animals following RT targeting with shRNA-*Scn8a* compared to either TC targeting with shRNA-*Scn8a* or RT targeting with shRNA-Scram (Figures 6B and 6C; Seizures per hour; one-way ANOVA, Tukey post hoc test, \* $p < 0.05$ , RT-targeted shRNA-

Scram,  $0.8 \pm 0.5$ , TC-targeted shRNA-*Scn8a*,  $1.5 \pm 0.3$ , RT targeted shRNA-*Scn8a*,  $14.5 \pm 1.3$ ).

### DISCUSSION

Using cell-type- and region-specific genetic manipulations of *Scn8a* and electrophysiology, we show that the seizure-protective and ictogenic consequences of reduced *Scn8a* activity can be decoupled and respectively attributed to distinct alterations in cortical and thalamic networks. Specifically, we found that loss of *Scn8a* from cortical excitatory neurons increases seizure resistance and the lifespan of epileptic animals. In contrast, loss of *Scn8a* from inhibitory neurons of the thalamic reticular nucleus (RT) is sufficient to cause hypersynchrony of the thalamocortical system and spontaneous absence seizures. This hypersynchrony is explained by specific intrinsic and synaptic deficits that we observed in RT neurons. First, loss of *Scn8a* was found to preferentially affect asynchronous tonic firing of RT cells.

Second, loss of *Scn8a* led to activity-dependent reductions in desynchronizing recurrent RT inhibition. Together, these results highlight a previously unrecognized importance of *Scn8a* in regulating thalamocortical network states, define a novel mechanism of absence seizure generation, and reveal a path for targeting *Scn8a* to achieve seizure control without risking the development of absence epilepsy.

### **Scn8a Channels Regulate Cortical Excitation and Convulsive Seizure Susceptibility**

We previously reported that mutations that reduce the expression or activity of *Scn8a* increase seizure resistance and ameliorate seizure phenotypes in *Scn1a* epilepsy models (Hawkins et al., 2011; Makinson et al., 2014, 2016; Martin et al., 2007). Here we show that selective deletion of *Scn8a* in excitatory, but not inhibitory, neurons is sufficient to protect against induced seizures and hippocampal epileptiform bursts, reduce cortical pyramidal cell excitability, and increase seizure resistance in an *Scn1a* epileptic mutant (Figures 1, S3, and S4). Based on our findings, we propose that *Scn8a* is a potent regulator of neocortical and hippocampal glutamatergic excitation and thus could potentially be targeted to achieve seizure control.

The cortical hypoexcitability model of *Scn8a*-mediated seizure resistance is consistent with the findings described here, with previous reports associating reduced *Scn8a* activity with seizure protection (Hawkins et al., 2011; Makinson et al., 2014; Martin et al., 2010), and with the observation that certain anticonvulsant drugs reduce VGSC activity and cortical cell AP generation. *Scn8a* seizure protection however is seemingly at odds with reports linking *Scn8a* mutations to epileptic encephalopathy (EE) (Larsen et al., 2015; Veeramah et al., 2012). As such, we propose that *Scn8a* is a bidirectional regulator of cortical excitation, which can be tuned up or down to increase or decrease seizure susceptibility. In support of this view, many human EE patients carry point mutations in *SCN8A* that are either known or suspected to be gain of function (GOF) (Meisler et al., 2016; Veeramah et al., 2012), and pathologies that are associated with increased *Scn8a* channel expression are also associated with increased seizure risk (Blumenfeld et al., 2009; Hargus et al., 2011; Sun et al., 2013). The *Scn8a* manipulations reported here are designed to reduce channel expression (Figure S1). Consistent with this general principle, a mutation in *Scn8a* with both GOF and loss-of-function (LOF) properties exhibits a complex seizure phenotype displaying both pro- and anticonvulsant phenotypes (Makinson et al., 2016).

While *Scn1a* and *Scn8a* are both expressed in cortical inhibitory neurons (Dutton et al., 2013; Lorincz and Nusser, 2008; Ogiwara et al., 2007; Papale et al., 2013; Yu et al., 2006), in sharp contrast to the severe epilepsy that occurs following deletion of *Scn1a* in interneurons (Cheah et al., 2012; Dutton et al., 2013), *Scn8a* deletion in inhibitory neurons (via *Ppp1r2* or *Dlx5/6*) produced neither convulsive seizures nor increased susceptibility to fluorothyl-induced generalized tonic-clonic seizures (Figure 1A). It follows that co-segregation of *Scn1a* and *Scn8a* mutant alleles can exert opposing influences on excitatory and inhibitory components of the cortical network to approximate normal levels of excitability.

### **Thalamic Hypersynchrony by Loss of Scn8a**

Absence epilepsy is characterized by the occurrence of spontaneous cortical spike-and-wave discharges (SWDs) accompanied by loss of consciousness (Kostopoulos, 2001). These seizures are pathological episodes of hypersynchronous activity within the thalamocortical system, which normally functions to mediate thalamic processes (Beenhakker and Huguenard, 2009; Jones, 2009; Pinault, 2004; Steriade et al., 1993).

Mutations in *Scn8a* are associated with absence epilepsy in mice and humans (Berghuis et al., 2015; Papale et al., 2009). In order to identify the cell types and brain regions that mediate *Scn8a*-absence epilepsy, we generated mice with restricted deletion of *Scn8a* and analyzed ECoG activity for evidence of absence seizures. Neither genetic deletion of the *Scn8a* gene in excitatory neurons using *Emx1* or *Camk2a Cre* transgenic lines, nor deletion of *Scn8a* from select inhibitory cells outside of the thalamus using the *Ppp1r2 Cre* line, produced absence seizures (Figure 1). However, broad deletion of *Scn8a* from inhibitory cells using the *Dlx5/6 Cre* line was necessary to induce absence epilepsy (Figure 1). These observations implicate RT, a subcortical structure that is entirely composed of inhibitory neurons and is robustly targeted by the *Dlx5/6 Cre* line (Figure S2; Table S2), in *Scn8a*-absence seizure generation; however, this approach did not exclude the possibility that *Scn8a*-absence seizures might also result from modulation of the thalamocortical system by other inhibitory inputs.

In order to evaluate the possibility that *Scn8a*-absence seizures originate from deficits in thalamic circuitry, we recorded multiunit activity in horizontal slices that preserve the RT-TC-RT loop, while inputs from the functionally connected cortex are severed (Huntsman et al., 1999; Kleiman-Weiner et al., 2009; Paz et al., 2011). Thus, electrical stimulation delivered to these severed cortical axons can contribute to the initiation of evoked activity within the RT-TC-RT loop but not to the maintenance of the ongoing oscillation. We found that isolated thalamic slices from *Scn8a*-deficient animals were capable of generating spontaneous hypersynchronous oscillations and prolonged evoked oscillations. We furthermore found that *Scn8a*-absence seizures involve strong thalamic activation in vivo by recording LFP and multiunit activity in the cortex and thalamus of awake, behaving, animals. Interestingly, reduced multiunit activity was observed in the thalamus for approximately 1 s preceding each seizure. Also, seizure clustering was apparent (Figure S5). Together, these findings indicate that certain thalamic network states are more favorable for *Scn8a*-absence seizure generation and that seizure onset may be predicted by identifying signatures of thalamic network activity.

To directly test whether the thalamus is sufficient to generate absence seizures, we selectively reduced *Scn8a* expression in RT using an RNAi approach. Knockdown of *Scn8a* expression in RT cells substantially increased absence seizure generation. These results are consistent with our measurement of isolated thalamic network activity in vitro and together indicate that impairment of RT cells by loss of *Scn8a* is sufficient to drive hypersynchrony in the thalamocortical system. Of note, we

reduced *Scn8a* expression in wild-type adult mice (2 month old), which developed with normal *Scn8a* function and expression prior to knockdown of *Scn8a*. This suggests that the mechanisms underlying absence seizure genesis can readily occur within the thalamic circuitry and are not developmentally regulated.

Previously, studies in isolated cortex and focal pharmacologic manipulations have shown that spike-wave events do not necessarily depend on thalamic input (Marcus and Watson, 1966; Steriade and Contreras, 1998), while lesioning of the thalamus (Avanzini et al., 1993) and alteration of the pattern of thalamic activity using optogenetics (Sorokin et al., 2017) have shown that the thalamus can be targeted to reduce seizures. Our observation that a genetic manipulation of a single gene in one thalamic cell type in adult wild-type mice is sufficient to cause spike-wave discharges demonstrates that thalamic alterations, in addition to cortex (Marcus and Watson, 1966; Steriade and Contreras, 1998), can lead to absence seizure generation.

Interestingly, fewer absence seizures were observed in animals with both excitatory and inhibitory cell deletion of *Scn8a* compared to animals with inhibitory cell deletion alone. This result demonstrates that loss of *Scn8a* from cortical excitatory neurons reduces susceptibility to absence seizures. *Scn8a* is known to be abundantly expressed in cortical projection neurons (Lorincz and Nusser, 2008), where it is important for supporting intrinsic and network excitability (Makinson et al., 2016; Makinson et al., 2014; Royeck et al., 2008). Within the thalamocortical system, CT cells project to both RT and TC cells, and CT input has been shown to be important for driving thalamic excitation and rhythmogenesis (Paz et al., 2011). As a result, reduced cortical *Scn8a* expression and therefore CT excitation would be expected to reduce thalamic excitation. Similarly, conditional deletion of the calcium channel *Cacna1a* in cortical projection neurons and in interneurons resulted in a less severe seizure phenotype than that produced by only inactivating the channel in interneurons (Rossignol et al., 2013). In either case, loss of *Scn8a* or *Cacna1a* channel expression in cortical projection cells reduces thalamocortical network synchronization and absence seizures. Thus, in mice that have a global reduction of *Scn8a* activity, competing pro- and anti-oscillatory influences overall favor hypersynchrony and the generation of absence seizures.

### Contribution of VGSCs to RT AP Firing Modes

During absence seizures, RT neurons produce bursts of activity that strongly inhibit TC neurons. This phasic inhibitory input from RT onto TC supports thalamocortical oscillations as strong hyperpolarization drives T-type  $\text{Ca}^{2+}$  channel-mediated post-inhibitory rebound bursts of TC cells (Beenhakker and Huguenard, 2009; Huguenard, 1996; von Krosigk et al., 1993; von Krosigk et al., 1999; Warren et al., 1994). In contrast, tonic RT outputs are thought to be desynchronizing, by interrupting periods of coordinated TC output (Sorokin et al., 2017). We and others have shown that mutations in *Scn8a* reduce spike firing in cortical excitatory and inhibitory neurons (Makinson et al., 2016; Royeck et al., 2008), whereas in the thalamus, the related VGSC gene *Scn1a* has been shown to reduce burst and tonic firing of RT

cells (Kalume et al., 2015). In contrast, loss of *Scn8a* in RT had less effect on bursting compared to tonic firing modes, with the latter more severely affected (Figure 4). Interestingly, in many *Scn8a*<sup>+/-</sup> RT cells, tonic mode firing was significantly reduced such that an initial burst of APs evoked by a strong depolarization that would normally be sufficient to drive sustained spiking instead produced an initial burst of APs followed by quiescence (Figure 4). We propose that shifting the balance of RT cell output from tonic toward bursts by loss of *Scn8a* would strengthen thalamic oscillations leading to absence seizures.

### Intra-RT Inhibition and Disruption by *Scn8a*

Rhythmic oscillations in the thalamus, like those we observed following loss of *Scn8a*, are inextricably tied to cycles of synaptic excitation and inhibition. The RT projects powerful synaptic inhibition onto most of the thalamus, and the RT→TC pathway is well studied and strongly implicated in thalamic rhythmogenesis (Cox et al., 1997; Huguenard and Prince, 1994; Steriade and Deschênes, 1984; von Krosigk et al., 1993). RT cells are also suspected to form recurrent inhibitory synapses with one another (RT→RT) and these have a desynchronizing influence on network activity by providing inhibition that is out of phase with the larger network oscillation (Bal et al., 1995; Deschênes et al., 1985; Huntsman et al., 1999; Lam et al., 2006; Sanchez-Vives and McCormick, 1997; Sohal and Huguenard, 2003; Sohal et al., 2006). These synapses are predicted to connect spatially distinct local subnetworks within the RT and may be important for sensory selection, attention, and cross-modal sensory integration (Ahrens et al., 2015; Makinson and Huguenard, 2015). However, direct evidence for this pathway has been elusive (Cruikshank et al., 2010; Hou et al., 2016; Parker et al., 2009). In order to develop a complete picture of synaptic excitation and inhibition in the TC↔RT loop, including RT inhibition, we developed a nuclei-specific assay of RT synaptic output by activating ultrafast channelrhodopsin (ChETA) specifically delivered to presynaptic RT cells while recording IPSCs in post-synaptic TC and RT cells. Using this approach, we characterized isolated RT→TC and RT→RT synapses, and we compared the relative strength of these synaptic components in *Scn8a*<sup>+/-</sup> animals with absence epilepsy. We found that RT→TC synaptic inhibition is robust and unaltered by loss of *Scn8a* (Figures 5D–5F), while *Scn8a*<sup>+/-</sup> RT→RT IPSCs are relatively small in amplitude and exhibit activity-dependent failure from 5 to 20 Hz (Figures 5D and 5E). Previous histological investigations of RT axons and synapses have shown that intra-RT fibers are relatively sparse and small diameter relative to the main axon trunk that extends to TC cells (Mulle et al., 1986; Sanchez-Vives et al., 1997). We therefore speculate that RT projecting axons and synapses are susceptible to presynaptic failure under certain pathological conditions including sodium channel dysfunction and high-frequency activation due to differences in their abundance and morphology. We propose that under conditions of high-frequency RT output, desynchronizing RT→RT synaptic inhibition breaks down, while synchronizing RT→TC synaptic inhibition is maintained (Figure 7B). Preferential loss of this desynchronizing component of the network allows strong rhythmic thalamic oscillations to persist, which then leads to the generation of

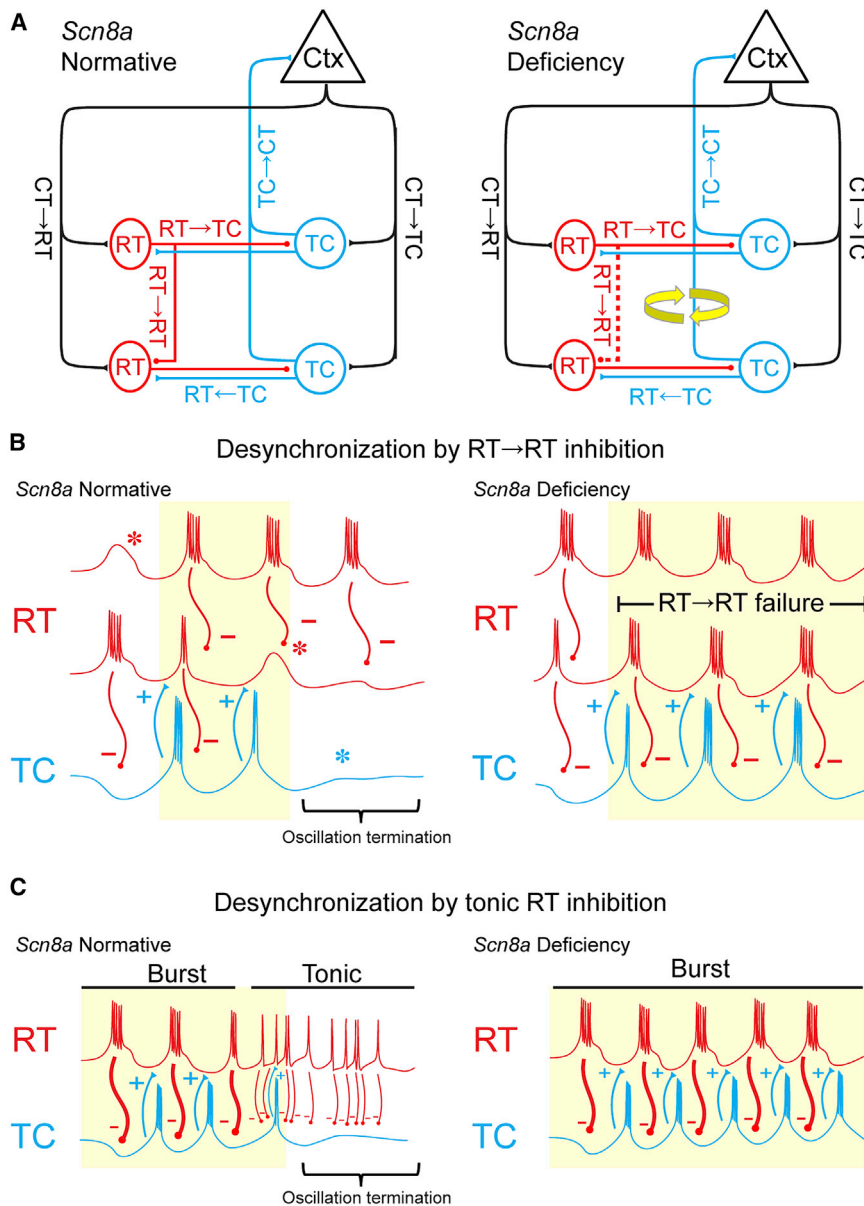


**Figure 7. Conceptual Model of *Scn8a*-Absence Seizure Generation**

(A) Illustrated are diagrams of normal and *Scn8a*-deficient thalamocortical circuits. The thalamocortical loop consists of reciprocally connected glutamatergic corticothalamic (CT, Blue) and thalamocortical (TC, black) neurons. The thalamic reticular nucleus (RT, red) forms inhibitory synapses with TC neurons (RT→TC) and also with RT neurons (RT→RT). *Scn8a* deficiency causes a breakdown in intra-RT inhibition (B) and a shift in the balance of tonic versus burst outputs of RT cells (C), which together cooperate to strengthen synchronous activity (A, yellow cycle).

(B) RT→RT synaptic activity (red inhibitory connections) typically function to sparsify RT cell bursting (asterisk) and weaken synchronous RT output. The latter is an important driver of post-inhibitory rebound bursting activity in TC cells (blue traces). TC cell bursting returns excitation to RT cells (blue excitatory connections), which drives another iteration of synchronous network activity (yellow background). *Scn8a*-deficient thalamic networks exhibit loss of RT→RT synaptic inhibition, particularly under conditions of high activity. Thus, rhythmic outputs are reinforced by loss of desynchronizing RT→RT inhibition.

(C) Loss of *Scn8a* preferentially reduces asynchronous tonic firing (thin red connections) of RT cells, while synchronizing phasic burst firing (thick red connections) is maintained, shifting the balance of tonic versus burst firing to favor phasic outputs. Tonic RT inhibition partially occurs out of phase with ongoing rhythmic activity (yellow background) and thereby would act to reduce network oscillations.

(A–C) We propose that these deficits coconspire to generate hypersynchrony in the thalamocortical system leading to absence seizures (1) by impairing the desynchronizing RT→RT synapse and (2) by shifting the balance of pro- and anti-oscillatory RT output modes toward the oscillatory state.

absence seizures (Figure 7). To our knowledge, these recordings are the first demonstration of a specific disruption in the intra-RT synapse that is associated with pathology.

### Overall Conclusions

We have identified distinct roles for *Scn8a* in hypoexcitation of cortical and hyperexcitation of thalamic circuits, which respectively underlie the seizure-protective and ictogenic properties associated with reduced *Scn8a* function. We document a novel mechanism of absence seizure generation in which selective loss of *Scn8a* from RT: (1) shifts the balance of tonic and burst output modes of RT cells and (2) impairs desynchronizing RT-RT synaptic inhibition (Figure 7). Our findings demonstrate for the first time that ion channel loss in RT

is sufficient to generate absence seizures in wild-type animals. These findings not only implicate *Scn8a* in pathological network states such as absence seizures, they also motivate future studies toward discerning the precise role of *SCN8A* in fundamental thalamic processes including sleep, sensation, attention, perception, and consciousness.

### STAR★METHODS

Detailed methods are provided in the online version of this paper and include the following:

- KEY RESOURCES TABLE
- CONTACT FOR REAGENTS AND RESOURCE SHARING

- **EXPERIMENTAL MODEL AND SUBJECT DETAILS**
  - Mouse Strains
- **METHOD DETAILS**
  - Genotyping of transgenic animals
  - Flurothyl seizure induction
  - In vivo ECoG and multiunit recordings
  - Adeno-associated viral constructs
  - Viral injection Procedures
  - Western blot analysis
  - Immunohistochemistry
  - In vitro slice electrophysiology
  - In vitro slice electrophysiology data acquisition and analysis
  - Optogenetic stimulation
- **QUANTIFICATION AND STATISTICAL ANALYSIS**

### SUPPLEMENTAL INFORMATION

Supplemental Information includes seven figures and two tables and can be found with this article online at <http://dx.doi.org/10.1016/j.neuron.2017.01.031>.

### AUTHOR CONTRIBUTIONS

Conceptualization, C.D.M., A.L.G., A.E., and J.R.H.; Methodology, C.D.M., B.S.T., J.M.S., and J.R.H.; Formal Analysis, C.D.M., B.S.T., J.M.S., and J.C.W.; Investigation, C.D.M., B.S.T., J.M.S., J.C.W., and C.A.C.; Resources, A.E. and J.R.H.; Writing, C.D.M., A.E., and J.R.H.; Visualization, C.D.M.; Supervision, A.L.G., A.E., and J.R.H.; Funding Acquisition, A.L.G., A.E., C.D.M., and J.R.H.; Co-senior authors, A.E., and J.R.H.

### ACKNOWLEDGMENTS

A.E. and J.R.H. contributed equally to this manuscript as co-senior authors. This research was supported by a postdoctoral training fellowship from the Epilepsy Foundation 299208 and NIH institutional epilepsy training program NS007280 (CDM), National Institutes of Health under awards numbers R01NS048336 (A.L.G.), R01NS065187 (A.E. and A.L.G.), R01NS034774 (J.R.H.), and R01NS072221 (A.E.). This study was supported in part by the NINDS core facilities grant P30NS055077 to the Emory University Microscopy Core. We would like to thank Dr. Miriam Meisler at the University of Michigan for providing the *Scn8a* floxed line, Dr. Kazu Nakazawa at the National Institutes of Health for providing the *Ppp1r2 Cre* line, and Dr. Ioannis Dragatsis at the University of Tennessee for providing the *Camk2a Cre* line.

Received: October 12, 2016

Revised: November 30, 2016

Accepted: January 30, 2017

Published: February 23, 2017

### REFERENCES

Ahrens, S., Jaramillo, S., Yu, K., Ghosh, S., Hwang, G.R., Paik, R., Lai, C., He, M., Huang, Z.J., and Li, B. (2015). ErbB4 regulation of a thalamic reticular nucleus circuit for sensory selection. *Nat. Neurosci.* **18**, 104–111.

Avanzini, G., Vergnes, M., Spreafico, R., and Marescaux, C. (1993). Calcium-dependent regulation of genetically determined spike and waves by the reticular thalamic nucleus of rats. *Epilepsia* **34**, 1–7.

Bal, T., von Krosigk, M., and McCormick, D.A. (1995). Role of the ferret perigeniculate nucleus in the generation of synchronized oscillations in vitro. *J. Physiol.* **483**, 665–685.

Bean, B.P. (2007). The action potential in mammalian central neurons. *Nat. Rev. Neurosci.* **8**, 451–465.

Beenhakker, M.P., and Huguenard, J.R. (2009). Neurons that fire together also conspire together: is normal sleep circuitry hijacked to generate epilepsy? *Neuron* **62**, 612–632.

Belforte, J.E., Zsiros, V., Sklar, E.R., Jiang, Z., Yu, G., Li, Y., Quinlan, E.M., and Nakazawa, K. (2010). Postnatal NMDA receptor ablation in corticolimbic interneurons confers schizophrenia-like phenotypes. *Nat. Neurosci.* **13**, 76–83.

Berghuis, B., de Kovel, C.G., van Iterson, L., Lamberts, R.J., Sander, J.W., Lindhout, D., and Koeleman, B.P. (2015). Complex SCN8A DNA-abnormalities in an individual with therapy resistant absence epilepsy. *Epilepsy Res.* **115**, 141–144.

Blumenfeld, H., Lampert, A., Klein, J.P., Mission, J., Chen, M.C., Rivera, M., Dib-Hajj, S., Brennan, A.R., Hains, B.C., and Waxman, S.G. (2009). Role of hippocampal sodium channel Nav1.6 in kindling epileptogenesis. *Epilepsia* **50**, 44–55.

Bryant, A.S., Li, B., Beenhakker, M.P., and Huguenard, J.R. (2009). Maintenance of thalamic epileptiform activity depends on the astrocytic glutamate-glutamine cycle. *J. Neurophysiol.* **102**, 2880–2888.

Cheah, C.S., Yu, F.H., Westenbroek, R.E., Kalume, F.K., Oakley, J.C., Potter, G.B., Rubenstein, J.L., and Catterall, W.A. (2012). Specific deletion of Nav1.1 sodium channels in inhibitory interneurons causes seizures and premature death in a mouse model of Dravet syndrome. *Proc. Natl. Acad. Sci. USA* **109**, 14646–14651.

Claes, L., Del-Favero, J., Ceulemans, B., Lagae, L., Van Broeckhoven, C., and De Jonghe, P. (2001). De novo mutations in the sodium-channel gene SCN1A cause severe myoclonic epilepsy of infancy. *Am. J. Hum. Genet.* **68**, 1327–1332.

Cox, C.L., Huguenard, J.R., and Prince, D.A. (1997). Nucleus reticularis neurons mediate diverse inhibitory effects in thalamus. *Proc. Natl. Acad. Sci. USA* **94**, 8854–8859.

Cruikshank, S.J., Urabe, H., Nurmikko, A.V., and Connors, B.W. (2010). Pathway-specific feedforward circuits between thalamus and neocortex revealed by selective optical stimulation of axons. *Neuron* **65**, 230–245.

Deschênes, M., Madariaga-Domich, A., and Steriade, M. (1985). Dendrodendritic synapses in the cat reticularis thalami nucleus: a structural basis for thalamic spindle synchronization. *Brain Res.* **334**, 165–168.

Dragatsis, I., and Zeitlin, S. (2000). CaMKIIalpha-Cre transgene expression and recombination patterns in the mouse brain. *Genesis* **26**, 133–135.

Dutton, S.B., Makinson, C.D., Papale, L.A., Shankar, A., Balakrishnan, B., Nakazawa, K., and Escayg, A. (2013). Preferential inactivation of *Scn1a* in parvalbumin interneurons increases seizure susceptibility. *Neurobiol. Dis.* **49**, 211–220.

Escayg, A., MacDonald, B.T., Meisler, M.H., Baulac, S., Huberfeld, G., An-Gourfinkel, I., Brice, A., LeGuern, E., Moulard, B., Chaigne, D., et al. (2000). Mutations of SCN1A, encoding a neuronal sodium channel, in two families with GEFS+2. *Nat. Genet.* **24**, 343–345.

Gorski, J.A., Talley, T., Qiu, M., Puellas, L., Rubenstein, J.L., and Jones, K.R. (2002). Cortical excitatory neurons and glia, but not GABAergic neurons, are produced in the *Emx1*-expressing lineage. *J. Neurosci.* **22**, 6309–6314.

Gunaydin, L.A., Yizhar, O., Berndt, A., Sohal, V.S., Deisseroth, K., and Hegemann, P. (2010). Ultrafast optogenetic control. *Nat. Neurosci.* **13**, 387–392.

Hargus, N.J., Merrick, E.C., Nigam, A., Kalmar, C.L., Baheti, A.R., Bertram, E.H., 3rd, and Patel, M.K. (2011). Temporal lobe epilepsy induces intrinsic alterations in Na channel gating in layer II medial entorhinal cortex neurons. *Neurobiol. Dis.* **41**, 361–376.

Hawkins, N.A., Martin, M.S., Frankel, W.N., Kearney, J.A., and Escayg, A. (2011). Neuronal voltage-gated ion channels are genetic modifiers of generalized epilepsy with febrile seizures plus. *Neurobiol. Dis.* **41**, 655–660.

Hébert, J.M., and McConnell, S.K. (2000). Targeting of cre to the *Foxg1* (BF-1) locus mediates loxP recombination in the telencephalon and other developing head structures. *Dev. Biol.* **222**, 296–306.

- Hippenmeyer, S., Vrieseling, E., Sigrist, M., Portmann, T., Laengle, C., Ladle, D.R., and Arber, S. (2005). A developmental switch in the response of DRG neurons to ETS transcription factor signaling. *PLoS Biol.* 3, e159.
- Holland, K.D., Kearney, J.A., Glauser, T.A., Buck, G., Keddache, M., Blankston, J.R., Glaaser, I.W., Kass, R.S., and Meisler, M.H. (2008). Mutation of sodium channel SCN3A in a patient with cryptogenic pediatric partial epilepsy. *Neurosci. Lett.* 433, 65–70.
- Hou, G., Smith, A.G., and Zhang, Z.W. (2016). Lack of intrinsic GABAergic connections in the thalamic reticular nucleus of the mouse. *J. Neurosci.* 36, 7246–7252.
- Huguenard, J.R. (1996). Low-threshold calcium currents in central nervous system neurons. *Annu. Rev. Physiol.* 58, 329–348.
- Huguenard, J.R., and Prince, D.A. (1994). Intrathalamic rhythmicity studied in vitro: nominal T-current modulation causes robust antioscillatory effects. *J. Neurosci.* 14, 5485–5502.
- Huntsman, M.M., Porcello, D.M., Homanics, G.E., DeLorey, T.M., and Huguenard, J.R. (1999). Reciprocal inhibitory connections and network synchrony in the mammalian thalamus. *Science* 283, 541–543.
- Jones, E.G. (2009). Synchrony in the interconnected circuitry of the thalamus and cerebral cortex. *Ann. N Y Acad. Sci.* 1157, 10–23.
- Kalume, F., Oakley, J.C., Westenbroek, R.E., Gile, J., de la Iglesia, H.O., Scheuer, T., and Catterall, W.A. (2015). Sleep impairment and reduced interneuron excitability in a mouse model of Dravet Syndrome. *Neurobiol. Dis.* 77, 141–154.
- Kleiman-Weiner, M., Beenhakker, M.P., Segal, W.A., and Huguenard, J.R. (2009). Synergistic roles of GABAA receptors and SK channels in regulating thalamocortical oscillations. *J. Neurophysiol.* 102, 203–213.
- Kohrman, D.C., Harris, J.B., and Meisler, M.H. (1996). Mutation detection in the med and medJ alleles of the sodium channel Scn8a. Unusual splicing due to a minor class AT-AC intron. *J. Biol. Chem.* 271, 17576–17581.
- Kostopoulos, G.K. (2001). Involvement of the thalamocortical system in epileptic loss of consciousness. *Epilepsia* 42 (Suppl 3), 13–19.
- Lam, Y.W., Nelson, C.S., and Sherman, S.M. (2006). Mapping of the functional interconnections between thalamic reticular neurons using photostimulation. *J. Neurophysiol.* 96, 2593–2600.
- Larsen, J., Carvill, G.L., Gardella, E., Kluger, G., Schmiedel, G., Barisic, N., Depienne, C., Brilstra, E., Mang, Y., Nielsen, J.E., et al.; EuroEPINOMICS RES Consortium CRP (2015). The phenotypic spectrum of SCN8A encephalopathy. *Neurology* 84, 480–489.
- Levin, S.I., and Meisler, M.H. (2004). Floxed allele for conditional inactivation of the voltage-gated sodium channel Scn8a (Nav1.6). *Genesis* 39, 234–239.
- Liao, Y., Deprez, L., Maljevic, S., Pitsch, J., Claes, L., Hristova, D., Jordanova, A., Ala-Mello, S., Bellan-Koch, A., Blazevic, D., et al. (2010). Molecular correlates of age-dependent seizures in an inherited neonatal-infantile epilepsy. *Brain* 133, 1403–1414.
- Lorincz, A., and Nusser, Z. (2008). Cell-type-dependent molecular composition of the axon initial segment. *J. Neurosci.* 28, 14329–14340.
- Makinson, C.D., and Huguenard, J.R. (2015). Attentional flexibility in the thalamus: now we're getting SOMwhere. *Nat. Neurosci.* 18, 2–4.
- Makinson, C.D., Tanaka, B.S., Lamar, T., Goldin, A.L., and Escayg, A. (2014). Role of the hippocampus in Nav1.6 (Scn8a) mediated seizure resistance. *Neurobiol. Dis.* 68, 16–25.
- Makinson, C.D., Dutt, K., Lin, F., Papale, L.A., Shankar, A., Barela, A.J., Liu, R., Goldin, A.L., and Escayg, A. (2016). An Scn1a epilepsy mutation in Scn8a alters seizure susceptibility and behavior. *Exp. Neurol.* 275, 46–58.
- Manning, J.P., Richards, D.A., and Bowery, N.G. (2003). Pharmacology of absence epilepsy. *Trends Pharmacol. Sci.* 24, 542–549.
- Marcus, E.M., and Watson, C.W. (1966). Bilateral synchronous spike wave electrographic patterns in the cat. Interaction of bilateral cortical foci in the intact, the bilateral cortical-callosal, and adiencephalic preparation. *Arch. Neurol.* 14, 601–610.
- Martin, M.S., Tang, B., Papale, L.A., Yu, F.H., Catterall, W.A., and Escayg, A. (2007). The voltage-gated sodium channel Scn8a is a genetic modifier of severe myoclonic epilepsy of infancy. *Hum. Mol. Genet.* 16, 2892–2899.
- Martin, M.S., Dutt, K., Papale, L.A., Dubé, C.M., Dutton, S.B., de Haan, G., Shankar, A., Tufik, S., Meisler, M.H., Baram, T.Z., et al. (2010). Altered function of the SCN1A voltage-gated sodium channel leads to gamma-aminobutyric acid-ergic (GABAergic) interneuron abnormalities. *J. Biol. Chem.* 285, 9823–9834.
- Meisler, M.H., Helman, G., Hammer, M.F., Fureman, B.E., Gaillard, W.D., Goldin, A.L., Hirose, S., Ishii, A., Kroner, B.L., Lossin, C., et al. (2016). SCN8A encephalopathy: Research progress and prospects. *Epilepsia* 57, 1027–1035.
- Monory, K., Massa, F., Egertová, M., Eder, M., Blaudzun, H., Westenbroek, R., Kelsch, W., Jacob, W., Marsch, R., Ekker, M., et al. (2006). The endocannabinoid system controls key epileptogenic circuits in the hippocampus. *Neuron* 51, 455–466.
- Mulle, C., Madariaga, A., and Deschênes, M. (1986). Morphology and electrophysiological properties of reticularis thalami neurons in cat: in vivo study of a thalamic pacemaker. *J. Neurosci.* 6, 2134–2145.
- Ogiwara, I., Miyamoto, H., Morita, N., Atapour, N., Mazaki, E., Inoue, I., Takeuchi, T., Itohara, S., Yanagawa, Y., Obata, K., et al. (2007). Nav1.1 localizes to axons of parvalbumin-positive inhibitory interneurons: a circuit basis for epileptic seizures in mice carrying an Scn1a gene mutation. *J. Neurosci.* 27, 5903–5914.
- Osorio, I., Reed, R.C., and Peltzer, J.N. (2000). Refractory idiopathic absence status epilepticus: A probable paradoxical effect of phenytoin and carbamazepine. *Epilepsia* 41, 887–894.
- Papale, L.A., Beyer, B., Jones, J.M., Sharkey, L.M., Tufik, S., Epstein, M., Letts, V.A., Meisler, M.H., Frankel, W.N., and Escayg, A. (2009). Heterozygous mutations of the voltage-gated sodium channel SCN8A are associated with spike-wave discharges and absence epilepsy in mice. *Hum. Mol. Genet.* 18, 1633–1641.
- Papale, L.A., Makinson, C.D., Christopher Ehlen, J., Tufik, S., Decker, M.J., Paul, K.N., and Escayg, A. (2013). Altered sleep regulation in a mouse model of SCN1A-derived genetic epilepsy with febrile seizures plus (GEFS+). *Epilepsia* 54, 625–634.
- Parker, P.R., Cruikshank, S.J., and Connors, B.W. (2009). Stability of electrical coupling despite massive developmental changes of intrinsic neuronal physiology. *J. Neurosci.* 29, 9761–9770.
- Paz, J.T., Bryant, A.S., Peng, K., Fenno, L., Yizhar, O., Frankel, W.N., Deisseroth, K., and Huguenard, J.R. (2011). A new mode of corticothalamic transmission revealed in the Gria4(-/-) model of absence epilepsy. *Nat. Neurosci.* 14, 1167–1173.
- Pinault, D. (2004). The thalamic reticular nucleus: structure, function and concept. *Brain Res. Brain Res. Rev.* 46, 1–31.
- Posner, E. (2006). Pharmacological treatment of childhood absence epilepsy. *Expert Rev. Neurother.* 6, 855–862.
- Raman, I.M., and Bean, B.P. (1997). Resurgent sodium current and action potential formation in dissociated cerebellar Purkinje neurons. *J. Neurosci.* 17, 4517–4526.
- Raman, I.M., Sprunger, L.K., Meisler, M.H., and Bean, B.P. (1997). Altered subthreshold sodium currents and disrupted firing patterns in Purkinje neurons of Scn8a mutant mice. *Neuron* 19, 881–891.
- Rossignol, E., van den Maagdenberg, A.M., Rudy, B., and Fishell, G. (2013). CaV 2.1 ablation in cortical interneurons selectively impairs fast-spiking basket cells and causes generalized seizures. *Ann. Neurol.* 74, 209–222.
- Royeck, M., Horstmann, M.T., Remy, S., Reitze, M., Yaari, Y., and Beck, H. (2008). Role of axonal Nav1.6 sodium channels in action potential initiation of CA1 pyramidal neurons. *J. Neurophysiol.* 100, 2361–2380.
- Sanchez-Vives, M.V., and McCormick, D.A. (1997). Functional properties of perigeniculate inhibition of dorsal lateral geniculate nucleus thalamocortical neurons in vitro. *J. Neurosci.* 17, 8880–8893.

- Sanchez-Vives, M.V., Bal, T., and McCormick, D.A. (1997). Inhibitory interactions between perigeniculate GABAergic neurons. *J. Neurosci.* *17*, 8894–8908.
- Sohal, V.S., and Huguenard, J.R. (2003). Inhibitory interconnections control burst pattern and emergent network synchrony in reticular thalamus. *J. Neurosci.* *23*, 8978–8988.
- Sohal, V.S., Pangratz-Fuehrer, S., Rudolph, U., and Huguenard, J.R. (2006). Intrinsic and synaptic dynamics interact to generate emergent patterns of rhythmic bursting in thalamocortical neurons. *J. Neurosci.* *26*, 4247–4255.
- Sorokin, J.M., Davidson, T.J., Frechette, E., Abramian, A.M., Deisseroth, K., Huguenard, J.R., and Paz, J.T. (2017). Bidirectional control of generalized epilepsy networks via rapid real-time switching of firing mode. *Neuron* *93*, 194–210.
- Steriade, M., and Contreras, D. (1998). Spike-wave complexes and fast components of cortically generated seizures. I. Role of neocortex and thalamus. *J. Neurophysiol.* *80*, 1439–1455.
- Steriade, M., and Deschenes, M. (1984). The thalamus as a neuronal oscillator. *Brain Res.* *320*, 1–63.
- Steriade, M., McCormick, D.A., and Sejnowski, T.J. (1993). Thalamocortical oscillations in the sleeping and aroused brain. *Science* *262*, 679–685.
- Sugawara, T., Tsurubuchi, Y., Agarwala, K.L., Ito, M., Fukuma, G., Mazaki-Miyazaki, E., Nagafuji, H., Noda, M., Imoto, K., Wada, K., et al. (2001). A missense mutation of the Na<sup>+</sup> channel alpha II subunit gene Na(v)1.2 in a patient with febrile and afebrile seizures causes channel dysfunction. *Proc. Natl. Acad. Sci. USA* *98*, 6384–6389.
- Sun, W., Wagnon, J.L., Mahaffey, C.L., Briese, M., Ule, J., and Frankel, W.N. (2013). Aberrant sodium channel activity in the complex seizure disorder of Celf4 mutant mice. *J. Physiol.* *591*, 241–255.
- Taddese, A., and Bean, B.P. (2002). Subthreshold sodium current from rapidly inactivating sodium channels drives spontaneous firing of tuberomammillary neurons. *Neuron* *33*, 587–600.
- Torrence, C.C.G. (1998). A practical guide to wavelet analysis. *Bull. Am. Meteorol. Soc.* *79*, 61–78.
- Veeramah, K.R., O'Brien, J.E., Meisler, M.H., Cheng, X., Dib-Hajj, S.D., Waxman, S.G., Talwar, D., Girirajan, S., Eichler, E.E., Restifo, L.L., et al. (2012). De novo pathogenic SCN8A mutation identified by whole-genome sequencing of a family quartet affected by infantile epileptic encephalopathy and SUDEP. *Am. J. Hum. Genet.* *90*, 502–510.
- von Krosigk, M., Bal, T., and McCormick, D.A. (1993). Cellular mechanisms of a synchronized oscillation in the thalamus. *Science* *261*, 361–364.
- von Krosigk, M., Monckton, J.E., Reiner, P.B., and McCormick, D.A. (1999). Dynamic properties of corticothalamic excitatory postsynaptic potentials and thalamic reticular inhibitory postsynaptic potentials in thalamocortical neurons of the guinea-pig dorsal lateral geniculate nucleus. *Neuroscience* *91*, 7–20.
- Wagnon, J.L., and Meisler, M.H. (2015). Recurrent and non-recurrent mutations of scn8a in epileptic encephalopathy. *Front. Neurol.* *6*, 104.
- Warren, R.A., Agmon, A., and Jones, E.G. (1994). Oscillatory synaptic interactions between ventroposterior and reticular neurons in mouse thalamus in vitro. *J. Neurophysiol.* *72*, 1993–2003.
- Yu, F.H., Mantegazza, M., Westenbroek, R.E., Robbins, C.A., Kalume, F., Burton, K.A., Spain, W.J., McKnight, G.S., Scheuer, T., and Catterall, W.A. (2006). Reduced sodium current in GABAergic interneurons in a mouse model of severe myoclonic epilepsy in infancy. *Nat. Neurosci.* *9*, 1142–1149.

## STAR★METHODS

## KEY RESOURCES TABLE

REAGENT or RESOURCE	SOURCE	IDENTIFIER
<b>Antibodies</b>		
Rabbit anti-Scn8a	Millipore	Cat# AB5580; RRID: AB_2314858
Rabbit anti-Nav1.6 (Scn8a)	Alomone	Cat# ASC-009; RRID: AB_2040202
Rabbit anti-Nav1.1	Millipore	Cat# AB5204; RRID: AB_91751
Mouse anti-Nav1.2	Neuromab	Cat# 75-024; RRID: AB_2184030
HRP-conjugated goat anti-rabbit	GE Healthcare	Cat# RPN4301
HRP-conjugated goat anti-mouse	Jackson Immuno Research	Code: 115-035-068; RRID: AB_2338505
HRP-conjugated goat anti-mouse	ThermoFisher	Cat# 31430; RRID: AB_228307
Monoclonal mouse anti-GAD67	Millipore	Cat# MAB5406; RRID: AB_2278725
Monoclonal mouse anti-GAD65/67	Santa Cruz Biotechnology	Cat# sc-365180; RRID: AB_10710523
Rabbit anti-GluR2	Millipore	Cat# AB1768-I; RRID: AB_2313802
Monoclonal mouse anti-GluR2	Neuromab	Cat# 75-002; RRID: AB_2232661
Biotinylated anti-rabbit IgG	Vector Laboratories	Cat# BA-1000; RRID: AB_2313606
Alexa Fluor 488 goat anti-mouse	Invitrogen	Cat# A-11001; RRID: AB_2534069
Alexa Fluor 594 goat anti-mouse	Invitrogen	Cat# A-11005; RRID: AB_2534073
Alexa Fluor 488 goat anti-rabbit	Invitrogen	Cat# A-11008; RRID: AB_143165
Alexa Fluor 594 goat anti-rabbit	Invitrogen	Cat# A-11037; RRID: AB_2534095
Monoclonal mouse anti-parvalbumin	Swant	Cat# PV235; RRID: AB_10000343
<b>Bacterial and Virus Strains</b>		
AAV-EF1a-DIO-ChETA-EYFP	University of North Carolina Vector Core	N/A
AAV-EF1a-DIO-EYFP	University of North Carolina Vector Core	N/A
AAV-shRNA-Scn8a-GFP	University of Pennsylvania Viral Vector Core	N/A
AAV-shRNA-Scram-GFP	University of Pennsylvania Viral Vector Core	N/A
<b>Chemicals, Peptides, and Recombinant Proteins</b>		
Fluorescein Avidin D	Vector Laboratories	Cat# A-2001; RRID: AB_2336455
Streptavidin-conjugated Alexa Fluor 555	Thermo Fisher	Cat# S21381; RRID: AB_2307336
SuperSignal West Pico Chemiluminescent Substrate	Thermo Fisher	Cat# 34080
Biocytin	Sigma-Aldrich	Cat# B4261
Gabazine	Abcam	Cat# SR95531
<b>Experimental Models: Organisms/Strains</b>		
C3Fe.Cg-Scn8amed/J	The Jackson Laboratory	Stock No: 003798; RRID: IMSR_JAX:003798
B6;129-Gt(ROSA)26Sortm1Joe/J	The Jackson Laboratory	Stock No: 008516; RRID: IMSR_JAX:008516
B6.Cg-Gt(ROSA)26Sortm9(CAG-tdTomato)Hze/J	The Jackson Laboratory	Stock No: 007909; RRID: IMSR_JAX:007909
Scn8a <sup>fl</sup> /fl	<a href="#">Levin and Meisler, 2004</a>	N/A
C57BL/6J	The Jackson Laboratory	Stock No: 000664; RRID: IMSR_JAX:000664
129(Cg)-Foxg1tm1(cre)Skm/J	The Jackson Laboratory	Stock No: 004337; RRID: IMSR_JAX:004337
B6.129S2-Emx1tm1(cre)Krj/J	The Jackson Laboratory	Stock No: 005628; RRID: IMSR_JAX:005628
Tg(dlx6a-cre)1Mekk/J	The Jackson Laboratory	Stock No: 008199; RRID: IMSR_JAX:008199
CamKIIa-Cre	<a href="#">Dragatsis and Zeitlin, 2000</a>	N/A

(Continued on next page)

<b>Continued</b>		
REAGENT or RESOURCE	SOURCE	IDENTIFIER
Ppp1r2-Cre	<a href="#">Belforte et al., 2010</a>	N/A
B6;129P2-Pvalbtm1(cre)Arbr/J	The Jackson Laboratory	Stock No: 008069; RRID: IMSR_JAX:008069
Oligonucleotides		
Flox F (5'-GTG TGT GAT TCT CAA CAG TGG GTT-3'); Flox R (5'-GTC TGT AAG AAG GCC TGA AAG TGA-3')	<a href="#">Levin and Meisler, 2004</a>	N/A
Cre F (5'-TGA CCC GGC AAA ACA GGT AGT TA-3'); Cre R (5'-TTC-CCG-CAG-AAC-CTG-AAG-ATG-TT-3')	This Paper	N/A
DlxCre F (5'-AAATTGCCGAGGAGAGTGAA-3'); DlxCre R (5'-TCTGCAGTTCGAGTTGTTGG-3')	This Paper	N/A
Wild type F (5'-TCA GGA GCA AGG TTC TAG GC-3'), Common R (5'- AGG AGT GGC GCT AAA TCT GA-3'), and Med F (5'- TAC CAA AAG TCC CCA TAC CC-3')	The Jackson Laboratory	Jax Primer Numbers, 19574, 19575, 19576
Software and Algorithms		
ImageJ	Rasband, W.S., ImageJ, U. S. National Institutes of Health, Bethesda, Maryland	<a href="http://imagej.nih.gov/ij/">http://imagej.nih.gov/ij/</a>
Metamorph Imaging Software	Molecular Devices	<a href="https://www.moleculardevices.com/systems/metamorph-research-imaging/metamorph-microscopy-automation-and-image-analysis-software">https://www.moleculardevices.com/systems/metamorph-research-imaging/metamorph-microscopy-automation-and-image-analysis-software</a>
Imaris	Bitplane Scientific	<a href="http://www.bitplane.com/imaris/imaris">http://www.bitplane.com/imaris/imaris</a>
MBF Stereo Investigator	MBF Bioscience	<a href="http://www.mbfioscience.com/stereo-investigator">http://www.mbfioscience.com/stereo-investigator</a>
Prism	Graphpad Software Inc	<a href="https://www.graphpad.com/scientific-software/prism/">https://www.graphpad.com/scientific-software/prism/</a>
MATLAB	MathWorks	<a href="https://www.mathworks.com/">https://www.mathworks.com/</a>
Wdetecta	Custom Software, John R. Huguenard	<a href="https://huguenard-lab.stanford.edu/wdetecta.php">https://huguenard-lab.stanford.edu/wdetecta.php</a>
pClamp	Molecular Devices	<a href="https://www.moleculardevices.com/systems/conventional-patch-clamp/pclamp-10-software">https://www.moleculardevices.com/systems/conventional-patch-clamp/pclamp-10-software</a>
SigmaPlot	Systat Software Inc	<a href="http://www.sigmaplot.co.uk/products/sigmaplot/sigmaplot-details.php">http://www.sigmaplot.co.uk/products/sigmaplot/sigmaplot-details.php</a>
GenEx 5	Multi D	<a href="http://genex.gene-quantification.info/">http://genex.gene-quantification.info/</a>
GPower	Heinrich Heine Universität Düsseldorf	<a href="http://www.gpower.hhu.de/">http://www.gpower.hhu.de/</a>
Other		
Stellate Harmonie Routine EEG System	Natus Neurology	<a href="http://natus.com/documents/Stellate_Natus_HarmonieRoutineEEG_Final.pdf">http://natus.com/documents/Stellate_Natus_HarmonieRoutineEEG_Final.pdf</a>
32 channel, low noise recording system	Tucker-Davis Technologies	<a href="http://www.tdt.com/neurophysiology.html">http://www.tdt.com/neurophysiology.html</a>

## CONTACT FOR REAGENTS AND RESOURCE SHARING

Further information and requests for resources and reagents should be directed and will be fulfilled by the Lead Contact, John R. Huguenard ([huguenar@stanford.edu](mailto:huguenar@stanford.edu)).

## EXPERIMENTAL MODEL AND SUBJECT DETAILS

All experimental procedures were performed in accordance with the guidelines of the Institutional Animal Care and Use Committees of Emory University, the University of California, Irvine, and Stanford University.

## Mouse Strains

Mice carrying each *Cre* transgene were crossed to the ROSA reporter line B6;129-Gt(ROSA)26Sor<sup>tm1Joe</sup>/J or B6.Cg-Gt(ROSA)23or<sup>tm9(CAG-tdTomato)Hze</sup>/J. *Cre* expression induces deletion of an upstream floxed stop sequence leading to induction of fluorescent reporter expression in cells that express *Cre* recombinase. *Scn8a*-floxed mice were a kind gift from Dr. Miriam Meisler at the University of Michigan, Ann Arbor (Levin and Meisler, 2004). Homozygous female *Scn8a*-floxed mice (*Scn8a*<sup>fl/fl</sup>), maintained on the C57BL/6J background, were crossed to five different *Cre* transgenic lines: FoxG1, 129(Cg)-Foxg1<sup>tm1(Cre)skm</sup>/J (Hébert and McConnell, 2000), *Emx1*, B6.129-*Emx1tm1(Cre)Krl*/J (Gorski et al., 2002), *Dlx5/6* (Monory et al., 2006), *CamKIIa* (Dragatsis and Zeitlin, 2000), and *Ppp1r2* (Belforte et al., 2010). The *Ppp1r2* and the *CamKIIa* lines were kind gifts from Dr. Kazu Nakazawa at the National Institutes of Health and Dr. Ioannis Dragatsis at the University of Tennessee, respectively. *Cre*-dependant optogenetic viral constructs were injected into parvalbumin *Cre* transgenic animals B6;129P2-*Pvalb*<sup>tm1(Cre)Arbr</sup>/J (Hippenmeyer et al., 2005). Each *Cre* transgenic line was maintained on the C57BL/6J background. Mice carrying the *Scn8a* loss of function mutation med (Kohrman et al., 1996) (C3HeB/FeJ-*Scn8a*<sup>med</sup>/J), referred to in this manuscript as *Scn8a*<sup>+/-</sup>, were purchased from the Jackson laboratory. All comparisons were made using male and female mice generated by the same cross. Mice use for experiments were 2-4 months of age unless otherwise specified. The mice were maintained on a 12 hr light/dark cycle. Food and water were available ad libitum.

## METHOD DETAILS

### Genotyping of transgenic animals

PCR identification of the *Scn8a* floxed allele was performed as previously described (Levin and Meisler, 2004) using the primer pair FloxF (5'-GTG TGT GAT TCT CAA CAG TGG GTT-3'); FloxR (5'-GTC TGT AAG AAG GCC TGA AAG TGA-3'). The *Cre* transgene was identified using a primer pair located within the *Cre* transgene: CreF (5'-TGA CCC GGC AAA ACA GGT AGT TA-3'); CreR (5'-TTC-CCG-CAG-AAC-CTG-AAG-ATG-TT-3'). The following primers were used to specifically identify the *Dlx5/6* *Cre* transgene: DlxCreF (5'-AAATTGCCGAGGAGAGTGAA-3'); DlxCreR (5'-TCTGCAGTTCGAGTTGTTGG-3'). The following primers were used to identify the *Scn8a*<sup>+/-</sup> allele Wild-type F (5'-TCA GGA GCA AGG TTC TAG GC-3'), Common R (5'-AGG AGT GGC GCT AAA TCT GA-3'), and Med F (5'-TAC CAA AAG TCC CCA TAC CC-3').

### Flurothyl seizure induction

Seizure induction was performed as previously described (Makinson et al., 2016; Martin et al., 2007). Briefly, mice were placed in a clear chamber. Flurothyl (2,2,2-trifluoroethyl ether, Sigma-Aldrich) was introduced at a rate of 20  $\mu$ l/min. The latencies to the first myoclonic jerk (MJ) and generalized tonic-clonic seizure (GTCS) were recorded. The MJ is defined as a jerking movement of the neck and shoulders sometimes associated with tail clonus. The GTCS is defined as complete loss of postural control associated with forelimb and hindlimb tonic-clonic movement.

### In vivo ECoG and multiunit recordings

Continuous real-time video and ECoG recordings and seizure detection were performed at P14 in a cohort of animals to track the development of absence seizures. Bilateral cortical screw electrodes were implanted into the skull above the somatosensory cortex. ECoG recordings of mice less than 21 days of age were performed for 2 hr per day so that pups could remain with the dam between recording periods. Pup ECoG recordings were collected and analyzed using the Stellate Harmonie Routine EEG system (Natus Neurology). All other ECoG and multi-unit (MU) implants were performed on mice greater than 2 months of age. For ECoG/MU recordings, mice were connected to our acquisition software via a custom headpiece that reduces movement artifacts and provides local signal amplification. ECoG and local field potential (LFP) signals were acquired and digitized using the PZ5 digitizer and RZ5 acquisition system (Tucker-Davis Technologies, FL) and sampled at 2441 Hz, while thalamic extracellular MU signals were simultaneously sampled at 24414 kHz. ECoG was obtained by bilaterally screwing small self-tapping screws into the skull over the somatosensory cortex. MU/LFP in each animal were acquired using a hand-built optrode containing four linearly arranged tungsten electrodes separated by  $\sim$ 250  $\mu$ m attached to a 200  $\mu$ m core optical fiber. We referenced and grounded all recorded channels to an ECoG electrode placed over the cerebellum. Recordings were performed from roughly 11:00AM – 2:00PM in a quiet room to minimize circadian and effects.

Following acquisition, ECoG/LFP data were first bandpass filtered between 1 and 100 Hz using a 6th-order butterworth filter and then z-normalized by their standard deviations, while thalamic MU signals were bandpass filtered between 300 and 6000 Hz. To quantify changes in the power distribution during seizures, we applied the continuous wavelet transform (CWT) to the ECoG/LFP signals with a Morlet mother wavelet, 10 octaves, and 7 suboctaves, which produced a detailed time-frequency decomposition of the original signals (Torrence, 1998). Seizures were detected by thresholding the full power spectrogram; events that lasted less than 2 s, greater than 30 s, or had maximum power outside of typical absence seizure spectrums were rejected. For each seizure, mean power from different frequency bands ( $\delta$ : 1-4,  $\theta$ : 4-6,  $\theta$ \_swd: 7-10,  $\beta$ : 10-20, and broadband: 1-20) was extracted, averaged in time across 6 time points for the duration of the seizure, and normalized to the total power in across these bands. Because the CWT over-represents low-frequencies due to the redundant overlapping convolutions at large wavelet scales, we normalized the wavelet coefficients prior to extracting power (Torrence, 1998).

### Adeno-associated viral constructs

Adeno-associated viral (AAV) constructs containing the ultrafast optogenetic control vector CHETA (AAV-EF1a-DIO-ChETA-EYFP) as well as yellow fluorescent protein (YFP) control virus (AAV-EF1a-DIO-EYFP) were purchased from the University of North Carolina Vector Core. Concentrated viral suspensions ranged from  $1 \times 10^9$  to  $1 \times 10^{12}$  infectious particles per milliliter. AAV constructs containing shRNA constructs were produced by the University of Pennsylvania Vector Core. A short hairpin construct designed to target *Scn8a* was placed downstream of the U6 promoter along with a GFP sequence (shRNA-*Scn8a*). Control virus was produced that contained scrambled sequence placed downstream of the U6 promoter in addition to GFP (shRNA-Scram). Viral titer of the shRNA-Scram and shRNA-*Scn8a* suspensions ranged from  $1 \times 10^8$  to  $1 \times 10^9$  infectious particles per milliliter.

### Viral injection Procedures

For optogenetic RT activation experiments, 2 month old PV-*Cre* mice were injected with either optogenetic AAV-EF1a-DIO-ChETA-EYFP or control AAV-EF1a-DIO-EYFP viruses under isoflurane anesthesia. Stereotaxic injections were performed using a 10  $\mu$ l microsyringe and 30 gauge beveled needle (WPI). Coordinates were chosen that are medial to RT in order to minimize the possibility of infecting PV-*Cre* positive cells that are outside of the thalamus. Injection coordinates were as follows, relative to bregma: anterior posterior (AP)  $-0.95$  mm, medialateral (ML)  $\pm 1.5$  mm, dorsal ventral (DV)  $-2.8$  and  $-3.4$  mm. 300  $\mu$ l of concentrated virus suspension were injected at each site at a rate of 0.12  $\mu$ l/min. After each injection, the syringe was left in place for 2 min to prevent backflow. Incisions were closed with tissue adhesive (Vetbond, 3M; St. Paul, NM), and the animal was allowed to recover under a heat lamp. Animals were sacrificed for patch-clamp recordings 2-3 months after injections.

For validation of shRNA and control viruses, mice were anesthetized by isoflurane inhalation, and then fixed in a stereotaxic apparatus (Kopf, Tujunga, CA). Four holes were drilled in the skull above each injection site. Injections were performed using a Hamilton 0.5  $\mu$ L microsyringe (model #75) and 30-gauge needle. Validation of shRNA-*Scn8a* knockdown was performed in the hippocampus because this region is a discrete brain region that is easily targeted by stereotaxic injection and is known to express high levels of *Scn8a* and the other major CNS VGSCs (Blumenfeld et al., 2009; Liao et al., 2010; Lorincz and Nusser, 2008; Makinson et al., 2014). Four injection sites were chosen to target the hippocampus at the following coordinates, from bregma: anteroposterior (AP),  $-1.9$  mm; medialateral (ML),  $\pm 1.1$  mm,  $\pm 2.1$  mm; dorsoventral (DV),  $-1.9$  mm. The syringe was lowered to  $-2.0$  mm, and then retracted to  $-1.9$  mm and left in place for 4 min. Virus solution (1.0  $\mu$ l) was injected into each site at a rate of 0.12  $\mu$ l/min. After each injection, the syringe was left in place for 4 min before being retracted. Incisions were closed with tissue adhesive (Vetbond, 3M; St. Paul, NM), and the animal was allowed to recover on a heating pad. Postoperative analgesic (ibuprofen, 0.1 mg/kg) was provided for 3 days in the drinking water. Two weeks after injection, animals were sacrificed. Whole hippocampi were removed and flash-frozen for immunoblotting.

For *Scn8a* shRNA knockdown experiments, male 2-month old C3H/FeJ mice were injected with shRNA-*Scn8a* or shRNA-Scram constructs and implanted for ECoG recordings as described above. The analgesia meloxicam (2 mg/kg) was administered (s.c.) at the beginning of each surgery. Six holes were drilled in the skull, 4 for ECoG electrode implantation, and 2 for AAV injections. Injections were performed using a Hamilton 0.5- $\mu$ l microsyringe and 30-gauge needle. RT was targeted using the following coordinates relative to bregma: anterior posterior (AP)  $-0.95$  mm, medialateral (ML)  $\pm 1.9$  mm, dorsal ventral (DV)  $-3.0$  and  $-3.5$  mm. 300  $\mu$ l of concentrated virus suspension were injected at each site. TC was targeted using the following coordinates, relative to bregma: AP  $-1.25$  mm, ML  $\pm 0.9$  mm, DV  $-3.0$  mm. 600  $\mu$ l of virus was injected per site. AAV constructs were injected at a rate of 0.12  $\mu$ l/min. After each injection, the syringe was left in place for 2 min to prevent backflow. Incisions were closed with tissue adhesive (Vetbond, 3M; St. Paul, NM), and the animal was allowed to recover on a heating pad. ECoG recordings were collected three weeks following AAV injections.

### Western blot analysis

Membrane-enriched whole-brain or hippocampal tissue homogenates (15-30  $\mu$ g) were subjected to SDS-PAGE electrophoresis as previously described (Makinson et al., 2014). After blocking in 5% milk, blots were incubated overnight at 4°C in either polyclonal rabbit anti- $\text{Na}_v1.6$  primary antibody (1:200, Millipore, Billerica, MA), polyclonal rabbit anti- $\text{Na}_v1.6$  (1:225, Alomone, Israel), polyclonal rabbit anti- $\text{Na}_v1.1$  (1:200, Millipore), or monoclonal mouse anti- $\text{Na}_v1.2$  (1:1000, Neuromab, Davis, CA). Blots were then incubated in either HRP-conjugated goat anti-rabbit secondary (1:10,000, GE Healthcare, United Kingdom), HRP-conjugated goat anti-mouse secondary (1:10,000, Jackson ImmunoResearch, West Grove, PA), or HRP-conjugated goat anti-rabbit secondary (Sigma, St. Louis, MO, 1:16,000) for 1 hr followed by washing in SuperSignal West Pico Chemiluminescent substrate (Thermo Fisher) and imaging. Blots were also probed using a monoclonal mouse anti- $\alpha$ -tubulin (1:10,000, Millipore) or monoclonal mouse anti-pan-cadherin (1:100,000, Sigma) antibody followed by HRP-conjugated goat anti-mouse secondary (1:10,000, Jackson ImmunoResearch) or HRP-conjugated goat anti-mouse secondary (Pierce, 1:26,000) for normalization of sample loading. Image quantification was performed using ImageJ software (NIH).

### Immunohistochemistry

Immunohistochemistry was performed in order to determine the cell type-specificity of the *Emx1* and *Dlx5/6 Cre* lines (Figure S2 and Table S2) and to measure  $\text{Na}_v1.6$  expression in cortical and thalamic interneuronal populations (Figures 3A and 3B). Animals

were transcardially perfused with ice-cold 1% paraformaldehyde (PFA) and then brains were removed and post fixed in 1% PFA for 2 hr at 4°C. Brains were then transferred to 30% sucrose solution in phosphate buffered saline (PBS) for four days before cryosectioning 45µm thick sections. Free-floating sections were incubated with polyclonal rabbit anti-GAD67 (1:200, Millipore), polyclonal rabbit anti-GluR2 (1:200, Millipore), monoclonal mouse anti-GAD65/67 (1:250, Santa Cruz Biotechnology), mouse anti-GluR2 (1:5000, Neuromab), or mouse anti-GAD67 (1:2000, Millipore) in conjunction with polyclonal rabbit anti-*Scn8a* (1:200, Millipore). Sections were incubated in secondary antibodies: biotinylated anti-rabbit IgG (1:300, Vector Laboratories) and fluorescein avidin D (1:300, Vector Laboratories), or Alexa Fluor 555 anti-mouse IgG (1:1000, Thermo Fisher) or AlexaFluor 488 goat anti-mouse (1:1000, Thermo Fisher). Negative controls included sections that were not incubated with primary antibody, sections from adult *Scn8a*<sup>-/-</sup> mice, and sections from P2-3 neonatal mouse pups that do not express detectable levels of Na<sub>v</sub>1.6. Cells were counted using Imaris (Bitplane Scientific solutions) or MBF bioscience stereology software. At minimum three different animals were included in each analysis.

Following slice physiology procedures performed on animals injected with optogenetic constructs, slices were post-fixed in 4% PFA for 24 hr at 4°C and then transferred to 30% sucrose in PBS for four days. Sections were then resectioned to 45µm. Free-floating sections were incubated overnight at 4°C in streptavidin-conjugated Alexa Fluor 555 (Thermo Fisher Scientific) at 1:500 dilution to label cells that were filled with biocytin (Sigma-Aldrich) during patch clamp recordings and anti-parvalbumin (Swant) 1:1000 dilution to identify RT neurons. Slices were then mounted and imaged with a spinning disk confocal microscope (Zeiss motorized Axiovert 200M) and Metamorph imaging software.

### In vitro slice electrophysiology

Mice were anesthetized with pentobarbital sodium (i.p., 55 mg/kg) or halothane and brains were removed and placed in cold (~4°C) oxygenated (95% O<sub>2</sub>/5% CO<sub>2</sub>) sucrose slicing solution containing (in mM): 234 sucrose, 11 glucose, 26 NaHCO<sub>3</sub>, 2.5 KCl, 1.25 NaH<sub>2</sub>PO<sub>4</sub>, 10 MgSO<sub>4</sub>, and 0.5 CaCl<sub>2</sub> (310 mOsm). For patch clamp physiology on *Scn8a*<sup>+/-</sup> and control littermates, three to four month old male mice were used. Horizontal thalamic slices containing RT and TC were prepared as previously described (Huguenard and Prince, 1994). Slices were incubated and continuously oxygenated in warm (~32°C) artificial cerebrospinal fluid (ACSF) containing (in mM): 10 glucose, 26 NaHCO<sub>3</sub>, 2.5 KCl, 1.25 NaHPO<sub>4</sub>, 1 MgSO<sub>4</sub>, 2 CaCl<sub>2</sub>, and 126 NaCl (298 mOsm) for 1 hr and then transferred to room temperature (~21-23°C) for at least 15 min prior to recording. Pipette solutions contained (in mM): 120 K-gluconate, 11 KCl, 1 MgCl<sub>2</sub>, 1 CaCl<sub>2</sub>, 10 HEPES, 1 EGTA, and pH was adjusted to 7.4 with KOH (290 mOsm). For current-clamp recordings of CA1 pyramidal neurons, 2-month old animals were used. Pipette solutions contained (in mM): 126 K-gluconate, 4 KCl, 10 HEPES, 2 Mg-ATP, 0.3 GTP-Tris, 10 phosphocreatine; pH was adjusted to 7.2 with KOH (290 mOsm). I-V plots were constructed from a series of current steps in 10 pA increments from 20 to 150 pA. Recordings were corrected for an estimated -15 mV liquid junction potential. I-V plots were constructed from a series of current steps in 20 pA increments from -140 to 140 pA from a holding potential of -75 mV. No difference in resting membrane voltage, membrane capacitance, or series resistance was observed between control and experimental groups. For voltage-clamp recordings of inhibitory synaptic events including ChETA-evoked IPSCs, the pipette solution contained (in mM): 135 CsCl, 10 HEPES, 10 EGTA, 2 MgCl, 5 QX-314, and pH adjusted to 7.4 with CsOH (290 mOsm). Cells were held at -75 mV throughout the recording unless otherwise specified. Extracellular hippocampal recordings were performed as previously described (Makinson et al., 2014). ChETA-evoked IPSCs were detected using custom software (Wdetecta, JRH). During voltage clamp recordings of RT cells in brains that were infected with ChETA, IPSCs could be distinguished reliably from direct ChETA currents by either of two methods. First, ChETA responses always reached their peak amplitude in RT cells within 5 ms after the initiation of the light pulse while evoked IPSCs reached peak amplitudes after 8 ms from the initiation of the light pulse. By only detecting responses with peak times occurring after 8 ms of each pulse but before the initiation of the next pulse in the train, ChETA currents were excluded from the analysis but not the evoked IPSCs (Figure S6E). Second, in some cells after recording evoked IPSCs, light pulses were applied while blocking GABAA receptors with 10 µM gabazine (Abcam). These sweeps were then used to subtract ChETA currents from the previous recordings.

Thalamic oscillations were recorded using P23-30 animals. 400 µm thick horizontal slices containing RT and somatosensory (TC) thalamus were prepared as previously described (Huguenard and Prince, 1994). Recordings were performed in a humidified oxygenated interface chamber at 34°C and superfused at a rate of 3 mL min<sup>-1</sup> with oxygenated ACSF (indicated above), supplemented with 0.3 mM glutamine (Bryant et al., 2009). Thalamic oscillations were evoked by applying square current pulses (250 µA, 50 µs duration) to the internal capsule (i.c.) once every 30 s via a bipolar tungsten microelectrode (50-100 kΩ, FHC). Extracellular potentials were recorded using a monopolar tungsten microelectrode (50-100 kΩ, FHC) positioned in the dorsal thalamus. Signals were amplified 10,000 times and band-pass filtered between 10 Hz and 3 kHz. Before applying electrical stimulation, a minimum of 5 min of recording was collected to assay spontaneous activity.

### In vitro slice electrophysiology data acquisition and analysis

Patch clamp recordings were collected with a Multiclamp 700A or 700B (Molecular Devices) amplifier and Digidata 1320 or 1550A digitizer and pClamp10.6 (Molecular devices). Recordings were sampled and filtered at 10 kHz. Analysis of action potentials and

synaptic activity was performed using custom MATLAB (MathWorks) software. Burst index (BI) values were calculated using the following formula:

$$BI = 1 - (B/B + T) \text{ where } B = \text{abs}(I_b)/\text{sqrt}(S_b) \text{ and } T = \text{abs}(I_t)/\text{sqrt}(S_t).$$

$I_b$  = burst current threshold (pA),  $I_t$  = tonic AP threshold (pA),  $S_b$  = burst

AP number/stim length (ms),  $S_t$  = tonic AP number/stim length (ms)

In vitro thalamic oscillation data processing and analysis was performed using custom MATLAB functions. First raw traces were differentiated and smoothed, baseline RMS values were calculated and used to detect spikes via threshold crossing. Only spikes that exceeded 3x baseline RMS were included. In vitro bursts were defined as events containing at least four spikes within 10 ms, oscillations were defined as periods containing at least two bursts within 600 ms. Peri-stimulus time histograms (PSTHs) included spikes from each sweep using a bin width of 10 ms.

### Optogenetic stimulation

One month following AAV-EF1a-DIO-ChETA-EYFP or control AAV-EF1a-DIO-EYFP injection into RT, mice were euthanized and fresh brain slices were prepared for patch clamp physiology as described above. RT neurons expressing ChETA were activated with 475 nm light using a 200  $\mu$ m diameter optical fiber (Thorlabs). We applied 2 ms pulses of light (power at fiber was 20 mW) at 2, 5, 10, 20, 30, and 50 Hz for 5 s to stimulate synaptic release. Under the same stimulation conditions, light-evoked synaptic responses were not observed in the AAV-EF1a-DIO-EYFP control slices.

### QUANTIFICATION AND STATISTICAL ANALYSIS

All bar graphs indicate the mean and all error bars represent  $\pm$  standard error of the mean (SEM). Statistical analyses were performed using SigmaPlot 11.0 software (Systat Software, Chicago, IL), Prism 6 (GraphPad Software, La Jolla, CA), Custom MATLAB programs (MathWorks, Natick, MA), and SigmaPlot (Systat Software, San Jose, CA). Intergroup variance was assessed by the Levene's test, and normality of continuous datasets was determined using the Shapiro-Wilk test. One-way analysis of variance (ANOVA) was used to compare groups of three or more while the Mann-Whitney U test was used to compare between two groups. *Post hoc* comparisons were performed using either the Dunnett's or Bonferroni test. Power analysis were performed to estimate group sizes using G-Power software (Heinrich Heine Universität Düsseldorf). Experimenters were blind to experimental groups during data collection and analysis. Animals from the same cross were used in all experiments to minimize possible variability of genetic background and environment. Whole-cell recordings were performed on animals of each group on alternating days. Extracellular slice recordings were performed on littermate pairs that were sliced at the same time. Recordings were alternated between each group throughout the day.